Plankton and nekton community structure in the vicinity of the South Sandwich Islands (Southern Ocean) and the influence of environmental factors

Cecilia M. Liszka [a,*], Sally E. Thorpe [a], Marianne Wootton [b], Sophie Fielding [a], Eugene J. Murphy [a], Geraint A. Tarling [a]

[a] *British Antarctic Survey, High Cross, Madingley Road, Cambridge, CB3 0ET, UK*
[b] *Marine Biological Association, The Laboratory, Citadel Hill, Plymouth, Devon, PL1 2PB, UK*

ABSTRACT

The South Sandwich Islands (SSI) are a biologically productive archipelago situated in the eastern Scotia Sea to the south of the eastward flowing Antarctic Circumpolar Current (ACC). The islands support important populations of higher predators, including several penguin species, seals and humpback whales. Despite this, the plankton ecology of the region has been little studied and information on mesoscale structure and environmental forcing of plankton ecology is particularly limited. We conducted a comprehensive oceanographic and net sampling campaign during the CCAMLR Area 48 Survey (January and February 2019), incorporating phytoplankton, mesozooplankton and macrozooplankton/nekton. Satellite chlorophyll-a (chl-a) data showed the development of a large bloom that was initiated two months prior to our study period at the south-eastern edge of the archipelago and propagated northwards along the eastern side, limited to the east by mesoscale features associated with the southern boundary of the ACC (SB). Multivariate cluster analysis revealed distinct mesoscale structure within the plankton community, with four spatially defined groups of phytoplankton and macrozooplankton/nekton, and three cluster groups of mesozooplankton. North of the SB, we found some spatial congruence between the three plankton assemblages, with a distinct, spatially coherent, cluster in each, corresponding to a warmer water community. Here, biomass was dominated by mesozooplankton, particularly calanoid copepods *Rhincalanus gigas*, *Calanus propinquus*, *C. simillimus* and Euchaetidae. The corresponding phytoplankton community was dominated by small diatoms, particularly *Thalassionema* spp., *Pseudo-nitzschia* spp., *Fragilariopsis* spp. and *Chaetoceros* spp., whilst *Themisto gaudichaudii*, *Euphausia triacantha* and myctophids were the major contributors to the macrozooplankton/nekton community. South of the SB, there was some spatial congruence between phytoplankton and macrozooplankton/nekton community structure on the western side of the archipelago, as well as on the eastern side that corresponded to the location of the bloom, but less association with mesozooplankton structure. Macrozooplankton/nekton structure was strongly driven by environmental conditions 1–2 months prior to the survey, including sea-ice distribution, surface phytoplankton concentration and productivity, whilst mesozooplankton was more tightly coupled to in-situ prevailing conditions such as surface temperature and integrated chl-a. Top-down pressure between trophic levels may have also had an influence on spatial patterns although direct evidence is lacking. Antarctic krill (*Euphausia superba*) was found with relatively low biomass at our net sampling sites (median biomass of 0.04 mg m^{-3} or <0.01 g m^{-2}) while myctophids and the euphausiid *Thysanoessa* spp. predominated. We suggest that the highly productive and species rich pelagic community of the SSI supports multiple trophic pathways, and that off-shelf these may operate independently of Antarctic krill.

1. Introduction

The South Sandwich Islands (SSI) are a biologically productive archipelago of eleven islands situated in the eastern Scotia Sea, ~500 km south-east of South Georgia and south of a major oceanographic front, the Southern Boundary (SB) of the Antarctic Circumpolar Current (ACC). The islands support an important number of higher predators, including half the world's population of chinstrap penguins (c. 1.3 million pairs), large breeding populations of macaroni, Adelie and gentoo penguins (Convey et al., 1999; Hart and Convey, 2018; Lynch et al., 2016), and modest populations of fur and elephant seals (Hart and Convey, 2018). The archipelago is bounded to the east by the hadal South Sandwich Trench and to the south by the Weddell Sea, and the islands are the emergent parts of the tectonically active South Sandwich subduction system (Leat et al., 2016). Oceanographically, the region is influenced by the eastward flow of the ACC to the north, and eastward and northward flow of waters originating around the southern Scotia arc and the Weddell Sea in the south. The islands are also strongly ice-influenced, with the mean winter sea-ice distribution extending to the islands' northerly limit.

Since their discovery in 1775 (Holdgate and Baker, 1979), there has been comparatively little work on the plankton ecology of the region. This is despite knowledge of the region's rich biodiversity which sustained a period of seal prospecting in the late 1800s, as well as a number of scientific expeditions including the Discovery expedition in 1931, investigations during the 1960s which predominantly addressed geology and terrestrial biology (Holdgate, 1963; Holdgate and Baker, 1979; Kemp et al., 1931), and more recent assessments (Convey et al., 1999; Hart and Convey, 2018) that have confirmed the SSI as host to an important number of higher predators. This led to the creation in 2012 (and update in 2018) of the South Georgia and South Sandwich Islands Marine Protected Area (SGSSI MPA) (GSGSSI, 2019; Trathan et al., 2014) to protect important populations of higher predators, and avoid interactions between the fishery and predator populations. Nevertheless, knowledge of the plankton community structure and ecology of the region remains remarkably sparse (Advisory Group to GSGSSI, 2018) and, in contrast to nearby South Georgia, regular krill and zooplankton surveys have not been carried out. This leaves a critical gap in our understanding of the marine ecosystem and of connectivity between trophic levels in the region.

The SSI were visited as part of the Commission for Conservation of Antarctic Marine Living Resources (CCAMLR) 2000 synoptic survey (Watkins et al., 2004), which assessed the mesozooplankton, krill and higher predator distribution of the Scotia Sea and Western Antarctic Peninsula (WAP) region. Analysis of large-scale distribution showed the SSI to have a distinctly different mesozooplankton community composition compared to other regions of the Weddell and Scotia seas, but to have similarities to the community found around the WAP (Ward et al., 2004). However, resolution of mesoscale distribution within the SSI region was not possible given the coarse scale of that survey, nor were connections between lower and higher trophic levels. As part of the CCAMLR Area 48 Survey (Krafft et al., 2021), a repeat of the CCAMLR 2000 synoptic survey, a more detailed investigation of the region was carried out. Within the present analysis, our objective is to examine the composition and distribution of phytoplankton, zooplankton and nekton communities around the SSI at the mesoscale level and consider the spatial congruence between these groups. Furthermore, we aim to identify the principal environmental influences on the ecology of phytoplankton, zooplankton and nekton in this region.

2. Material and methods

2.1. Field sampling and data collection

Biological samples and in situ environmental data were collected during research cruise DY098 on the RRS Discovery during austral summer 2019. Sampling was conducted at 19 stations along a series of four transects around the South Sandwich Islands (SSI) archipelago between 26th January and 7th February (Fig. 1). Stations were located between 20 and 267 km distance from the 200 m isobath and in water depths >1000 m (Fig. 1), therefore representing off-shelf conditions. Macrozooplankton/nekton and mesozooplankton were sampled with an RMT8+1 (Rectangular Midwater Trawl opening and closing net (Baker et al., 1973; Piatkowski et al., 1994), equipped with nets of 8 m^2 and 1 m^2 mouth area, and 5 mm and 300 μm mesh, respectively). For the purposes of this paper, we refer to all organisms caught by the RMT8 net as macrozooplankton/nekton, and organisms caught by the RMT1 net as mesozooplankton. Nets were deployed obliquely to 200 m and depth-stratified samples were taken over 200-100 m and 100-0 m at each station. Stations were sampled every 12 h and so alternated between whether they were sampled during hours of daylight or darkness. Once on deck, excess water was eliminated and the contents of the RMT8 were weighed, sorted by species/taxon, enumerated and preserved in formalin (4% w/v). The contents of RMT1 nets were weighed and immediately preserved in formalin for later analysis.

At each RMT station, a Sea-Bird Scientific SBE 911 CTD (Sea-Bird Scientific, Bellevue, Washington) was deployed, collecting coincident oceanographic data including conductivity, temperature, and fluorescence. CTD data were processed according to standard British Oceanographic Data Centre (BODC) and BAS protocols (Fielding et al., 2019). Fluorescence was converted to chlorophyll-a using the manufacturer's calibration routine. Water samples for chlorophyll and phytoplankton analyses were collected from Niskin bottles closed at six depths (400 m, 200 m, 100 m, 50 m, 5 m and chlorophyll maximum (chl-max)). For chlorophyll, duplicate samples of 100 ml water from each depth were filtered onto a 25 mm ø glass fibre filter (GF/F), wrapped in tinfoil, and stored at −20 °C until later analysis. For phytoplankton, 200 ml water from each depth was collected directly into an amber glass bottle, fixed immediately with 2 ml Lugol's iodine, and stored in the dark at 4 °C until later analysis. Details of CTD and RMT deployments are given in Table 1.

Upon return to the home laboratory, chlorophyll filters were removed from the freezer, extracted in 10 ml 90% acetone for 24 h at −20 °C, and chlorophyll-a (chl-a) and phaeophytin-a (phaeo-a) were measured on a Turner Trilogy Fluorometer (Turner Designs, San Jose, USA) using the acidification module, in order to account for the presence of degradation products. A sub-sample of phytoplankton samples from the surface (5 m) and chl-max were analysed for phytoplankton and microzooplankton (heterotrophic organisms 20–200 μm in size). Cell identification and enumeration were conducted using standard Utermöhl methodology (Karlson et al., 2010), where 50 ml subsamples were settled for 24 h and examined under an inverted light microscope. Taxa were identified to species or genera where possible, or by group or size otherwise. Cell size categories of small and large represent cells <90 μm and >90 μm respectively, following Poulton et al. (2007). Where chains were encountered, all cells within each chain were treated as individual cells. Carbon biomass was estimated for the major phytoplankton groups, where available, by applying conversion factors, derived from published literature and database sources (Chitari and Anil, 2017; Leakey et al., 2002; Leblanc et al., 2012; Mathot et al., 2000; Poulton et al., 2007), to the abundance data. Conversion factors were not available for zooplankton, foraminifera, coccolithophores and Acantharia due to the substantial heterogeneity within these groups. As a result, all analyses are performed on abundances whilst carbon values are presented for indicative purposes.

Mesozooplankton from the RMT1 nets were sorted and enumerated by the Plankton Sorting and Identification Center Morski Instytut Rybacki (Gdynia, Poland). Common taxa were classified to species where possible; otherwise, samples were classified to the lowest possible taxonomic resolution. Raw macrozooplankton/nekton and mesozooplankton counts were divided by the water volume filtered (calculated as the oblique distance covered by the net based on the duration of the haul and ship speed and multiplied by the mouth area) to give
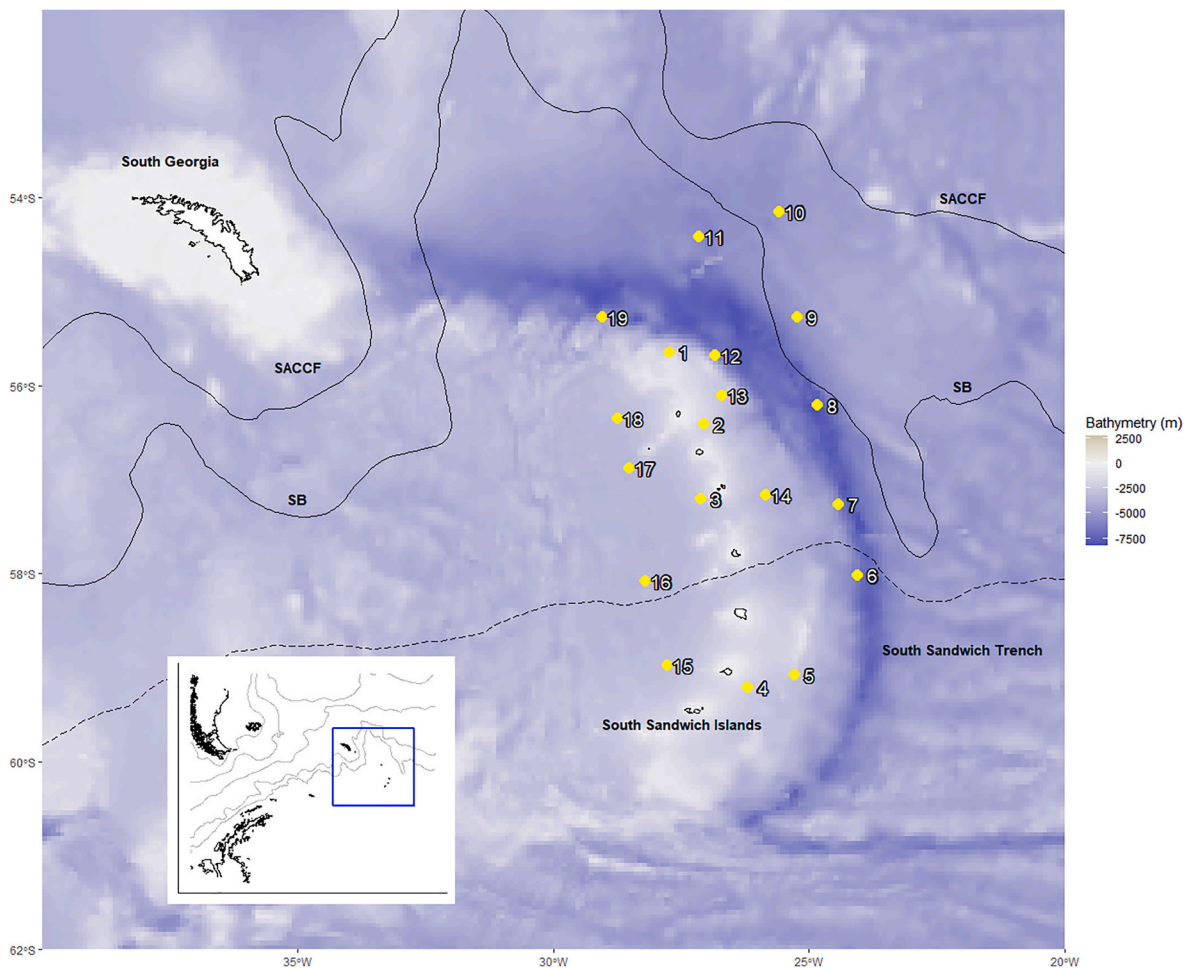
Fig. 1. Locations of stations occupied during the CCAMLR 2019 survey, shown as filled yellow circles around the South Sandwich Islands (SSI) archipelago. Station numbers correspond to the RMT net and CTD deployment details provided in Table 1. Solid black lines show the mean positions of the Southern Antarctic Circumpolar Current Front (SACCF) and southern boundary of the Antarctic Circumpolar Current (SB) (taken from Park and Durand, 2019). Also shown (black dashed line) is the mean sea ice extent for September 2018 (Fetterer et al., 2017, https://nsidc.org/data/G02135/versions/3). By February 2019, the sea ice had retreated south of the map domain. Bathymetry data are from GEBCO (https://www.gebco.net/data_and_products/gridded_bathymetry_data/). Inset shows the location of the SSI sampling region and mean frontal positions in the broader regional context.

individuals m^{-3}. Abundances were subsequently converted to biomass (mg m^{-3}) using conversion factors obtained from Ward et al. (2012) and Kiørboe (2013).

2.2. Environmental data

To investigate relationships between the zooplankton and its environment, a suite of environmental variables was obtained from satellite products or in-situ data (Supplementary Table 1).

Chlorophyll-a (chl-a), sea surface temperature (SST) and primary productivity (PP) for the period of the cruise and preceding time periods were obtained from satellite products (Supplementary Table 1) and averaged over the sampling period, or the previous month(s). Sea-ice data were obtained from the NSIDC sea ice concentration product, and distance to the ice edge was calculated using a standard threshold of 15% sea ice concentration to represent the sea ice edge (NSIDC, 2022) for the respective day of sampling with the contour and v.dist functions available in QGIS.

In-situ metrics related to SST, salinity and chl-a were also calculated from CTD data (Supplementary Table 1, Fig. 4). To investigate the potential influence of water mass characteristics, water mass categories were assigned to stations based on potential temperature-salinity plots (Fig. 3A). In addition, the maximum subsurface water temperature, depth of the maximum subsurface temperature, temperature minimum,

and the average temperature and salinity over the mixed layer were also derived from CTD data. The mixed layer depth (MLD), defined as a density difference relative to the surface of 0.05 kg m^{-3} (Venables et al., 2013), was calculated from temperature and salinity data from CTD profiles. In-situ chl-a and phaeophytin-a (phaeo-a) metrics were measured through pigment extraction from depth-discrete water samples (adapted from Yentsch and Menzel, 1963).

2.3. Data analysis and statistics

2.3.1. Analysis of phytoplankton community structure

Phytoplankton community structure was examined by carrying out a multivariate analysis on abundances from samples obtained from the chlorophyll maximum in PRIMER 7 (v7.0.13, Primer-E) (Clarke and Gorley, 2015). Abundance data were square root transformed to reduce the dominance of heavily abundant taxa, and the Bray-Curtis similarity was calculated. Group average hierarchical cluster analysis with similarity profiling (SIMPROF) and non-metric multidimensional scaling (nMDS) were carried out to determine statistically significant clustering and ordination of stations on the basis of the phytoplankton communities present. The SIMPER (similarity percentage) routine was used to evaluate which taxa, or groups of taxa, characterised resulting station clusters, and differentiated clusters from one another.

Table 1

Details of RMT net sampling and corresponding CTD stations, and key metrics of abundance and species richness (phytoplankton and zooplankton) and biomass (zooplankton). Date = date of deployment; D/N = day or night, as determined by sun angle; Species richness = total number of species per sample; Abundance = cells l^{-1} (phytoplankton) and individuals m^{-3} (zooplankton); Biomass = mg DW m^{-3} for both nets combined (zooplankton total biomass); mesozooplankton (RMT1); macrozooplankton/nekton (RMT8), with % contribution to total zooplankton biomass across both RMT nets given in brackets.

Station code	RMT station ID	CTD station ID	Lat	Long	Date	D/N	Phytoplankton species richness (# per sample)	Phytoplankton total abundance (cells l^{-1})	Zooplankton species richness (# per sample)	Zooplankton total abundance (inds m^{-3})	Zooplankton total biomass (mg m^{-3})	RMT1 biomass (mg m^{-3}) (%)	RMT8 biomass (mg m^{-3}) (%)
1	78	76	−55.64	−27.74	January 26, 2019	D	13	1,598,160	63	4.54	9.51	0.72 (7.6%)	8.78 (92.4%)
2	79	80	−56.41	−27.06	January 27, 2019	N	N/A	N/A	57	4.05	17.06	2.43 (14.2%)	14.63 (85.8%)
3	83	82	−57.21	−27.11	January 27, 2019	D	20	606,882	46	3.73	8.17	3.39 (41.5%)	4.78 (58.5%)
4	85	84	−59.21	−26.19	January 28, 2019	D	23	699,554	50	0.75	1.87	0.15 (7.9%)	1.72 (92.1%)
5	97	98	−59.08	−25.29	January 31, 2019	N	33	2,275,212	65	5.41	26.01	3.17 (12.2%)	22.84 (87.8%)
6	101	100	−58.02	−24.05	January 31, 2019	D	25	153,976	48	6.30	7.98	2.25 (28.1%)	5.73 (71.9%)
7	103	105	−57.26	−24.43	February 01, 2019	N	N/A	N/A	67	8.19	17.84	3.99 (22.4%)	13.85 (77.6%)
8	107	106	−56.21	−24.83	February 01, 2019	D	29	623,258	47	30.11	6.86	4.79 (69.9%)	2.06 (30.1%)
9	109	111	−55.27	−25.24	February 02, 2019	N	N/A	N/A	71	46.05	19.12	7.55 (39.5%)	11.57 (60.5%)
10	113	112	−54.15	−25.59	February 02, 2019	D	33	698,622	56	73.53	7.15	5.49 (76.8%)	1.66 (23.2%)
11	114	116	−54.42	−27.15	February 02, 2019	N	N/A	N/A	73	63.33	22.70	11.9 (52.4%)	10.8 (47.6%)
12	119	118	−55.68	−26.83	February 03, 2019	D	32	291,317	44	7.39	7.40	1.91 (25.9%)	5.49 (74.1%)
13	124	125	−56.10	−26.70	February 04, 2019	N	26	772,823	76	9.07	13.53	1.45 (10.7%)	12.08 (89.3%)
14	128	126	−57.17	−25.85	February 04, 2019	D	31	381,957	65	11.44	14.63	1.37 (9.3%)	13.27 (90.7%)
15	132	131	−58.98	−27.78	February 05, 2019	D	29	219,792	44	1.35	2.85	0.21 (7.3%)	2.64 (92.7%)
16	134	136	−58.09	−28.20	February 06, 2019	N	N/A	N/A	48	5.52	13.30	5.96 (44.8%)	7.35 (55.2%)
17	139	137	−56.88	−28.52	February 06, 2019	D	29	135,987	40	4.98	6.01	1.05 (17.5%)	4.96 (82.5%)
18	142	144	−56.35	−28.75	February 06, 2019	N	N/A	N/A	55	3.00	6.75	0.81 (12%)	5.94 (88%)
19	148	146	−55.27	−29.05	February 07, 2019	D	23	191,539	50	2.68	3.33	1.1 (33.1%)	2.23 (66.9%)

2.3.2. Analysis of zooplankton community structure

In order to minimise potential bias due to diel vertical migration (DVM) of the zooplankton, both depth strata (0–100 m and 100–200 m) were merged. For overall diversity metrics and descriptive statistics, meso- (RMT1) and macrozooplankton/nekton (RMT8) datasets were analysed as a combined dataset, with developmental stages aggregated up to the parent taxon and duplicates summed.

For multivariate analyses of zooplankton community structure, an initial analysis was carried out on the combined (RMT1 + RMT8) dataset. Based on this, and to determine the relative contributions of meso- and macrozooplankton/nekton to total zooplankton structure and biogeography, secondary analyses considered mesozooplankton and macrozooplankton/nekton datasets separately. To test whether any effect of day or night remained in each of these datasets, a one-way ANOSIM with Spearman rank correlation was performed across all samples.

As for the phytoplankton analysis, Bray-Curtis similarity was calculated on square root transformed data, and group average hierarchical cluster analysis with SIMPROF and nMDS were carried out, followed by SIMPER analysis. To establish which environmental variables best explained the observed zooplankton station groupings, a BIOENV analysis with Spearman rank correlation was carried out between the taxonomic and environmental data, aiming to maximise the rank correlation between the two respective resemblance matrices. Environmental variables were selected for consideration on the basis of factors including previously established or hypothesised relationships between different physical variables and ecological structure (e.g. measures of chl-a, phaeo-a or SST); examination of the role of static vs dynamic variables (e.g. bathymetric depth or distance to ice edge vs SST or PP); examination of the potential importance of deeper water mass properties (e.g. maximum subsurface temperature or temperature minimum); consideration of temporal lag in response (e.g. SST, PP or chl-a for different time periods); and consideration of data accessibility and replication by including comparisons of in situ versus remotely-sensed data (e.g. extracted chl-a or phaeo-a vs CTD fluorescence). Collinearity analysis was first performed to determine which variables were strongly correlated and should be removed from analysis, where correlation >0.8 was used as the cut-off and most commonly used variables were retained where there was a correlation. Remaining variables were checked for normality, transformed if necessary and normalised. All variables considered and retained are shown in Supplementary Table 1.

Analyses and statistics were carried out in PRIMER 7 (v7.0.13, Primer-E) (Clarke and Gorley, 2015), QGIS with GRASS v3.10.14 (QGIS Development Team, 2020) and R v3.6.2 (R Development Core Team, 2019).
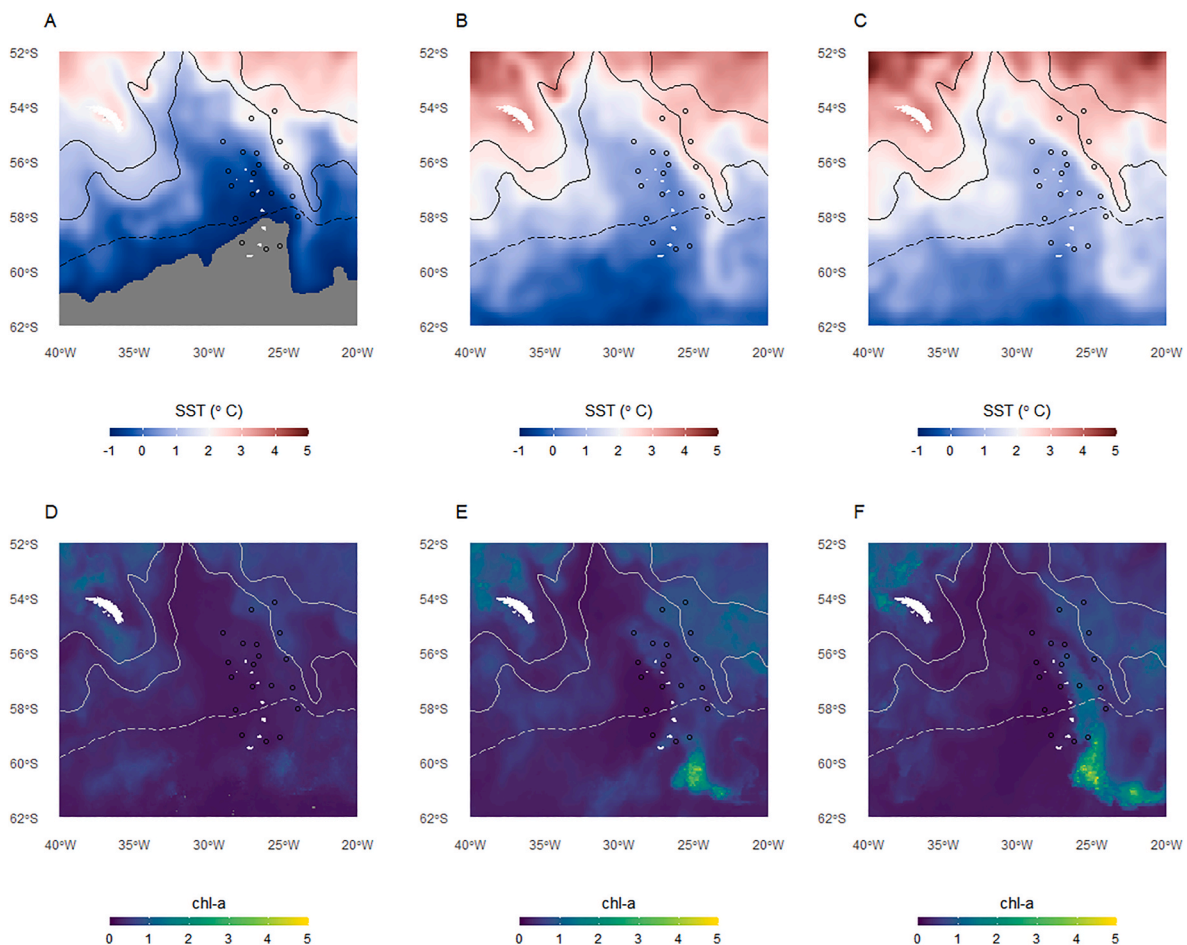

Fig. 2. Surface environmental conditions prior to and during the study period. A–C: mean SST (°C, 0.05 × 0.05° resolution) for the month prior to the study (26/11/2018–25/12/2018, A), one month prior to the study period (26/12/2018–25/01/2019, B) and during the study period (26/01/2019–07/02/2019, C). D–E: chl-a (μg l^{-1}, 4 km resolution) showing the development of the bloom from two months prior to the study period (dates as above, D), one month prior (E), and the study period (F). The dashed lines represent the winter (September 2018) ice-edge extent (daily average over 25 × 25 km resolution) (Fetterer et al., 2017, https://nsidc.org/data/G02135/versions/3). The summer (February 2019) ice-edge was further south than the map extent. Black circles show the location of sample stations. The solid lines represent the SACCF (north) and SB (south) (from Park and Durand, 2019).

3. Results

3.1. Large-scale environmental context

Two months prior to our study, sea ice was still covering the southern part of the SSI (Fig. 2A). This retreated rapidly over the subsequent month, and by the time of our study (late January 2019) was far south of 62 °S. Satellite imagery showed that SST transitioned from warmer waters in the north (ranging from 2 to 5 °C north of the mean location of the Southern Antarctic Circumpolar Current Front, SACCF) to colder waters in the south (ranging from −1 to ~1.5 °C south of the Southern Boundary of the ACC, SB). Between the two months prior to our study (November/December 2018) and the study period itself (January/February 2019), these broad patterns remained fairly consistent, although the surface waters became warmer as the summer progressed (Fig. 2A–C). Over the same period, surface chl-a indicated the development of a strong phytoplankton bloom. The bloom appeared to initiate at the south-eastern edge of the archipelago in the region opened up by the retreating ice (Fig. 2D). The bloom then propagated northwards along the eastern edge of the archipelago, and was putatively limited to the east by the circulation related to the SB (Fig. 2E–F). This bloom was spatially distinct from, and substantially higher in magnitude than, a region of elevated chl-a to the north of the SB. The series of satellite-derived chl-a values were highly correlated ($R^2 = 0.831$–0.976, $p < 0.0001$) with primary productivity (PP) for the corresponding time period. PP for December was also highly correlated with the distance to the ice edge ($R^2 = 0.844$, $p < 0.0001$). PP was therefore excluded from analyses.

3.2. In-situ environmental conditions

Maximum sea-ice extent during the previous winter reached ~56 °S in July 2018, encompassing 10 of our 19 stations (Fig. 2). During the study period, sea-ice had retreated south of 62 °S and distance to the prevailing ice-edge ranged from 1130 km to 1615 km.

A potential temperature-salinity (θ-S) plot over the upper 1000 m of
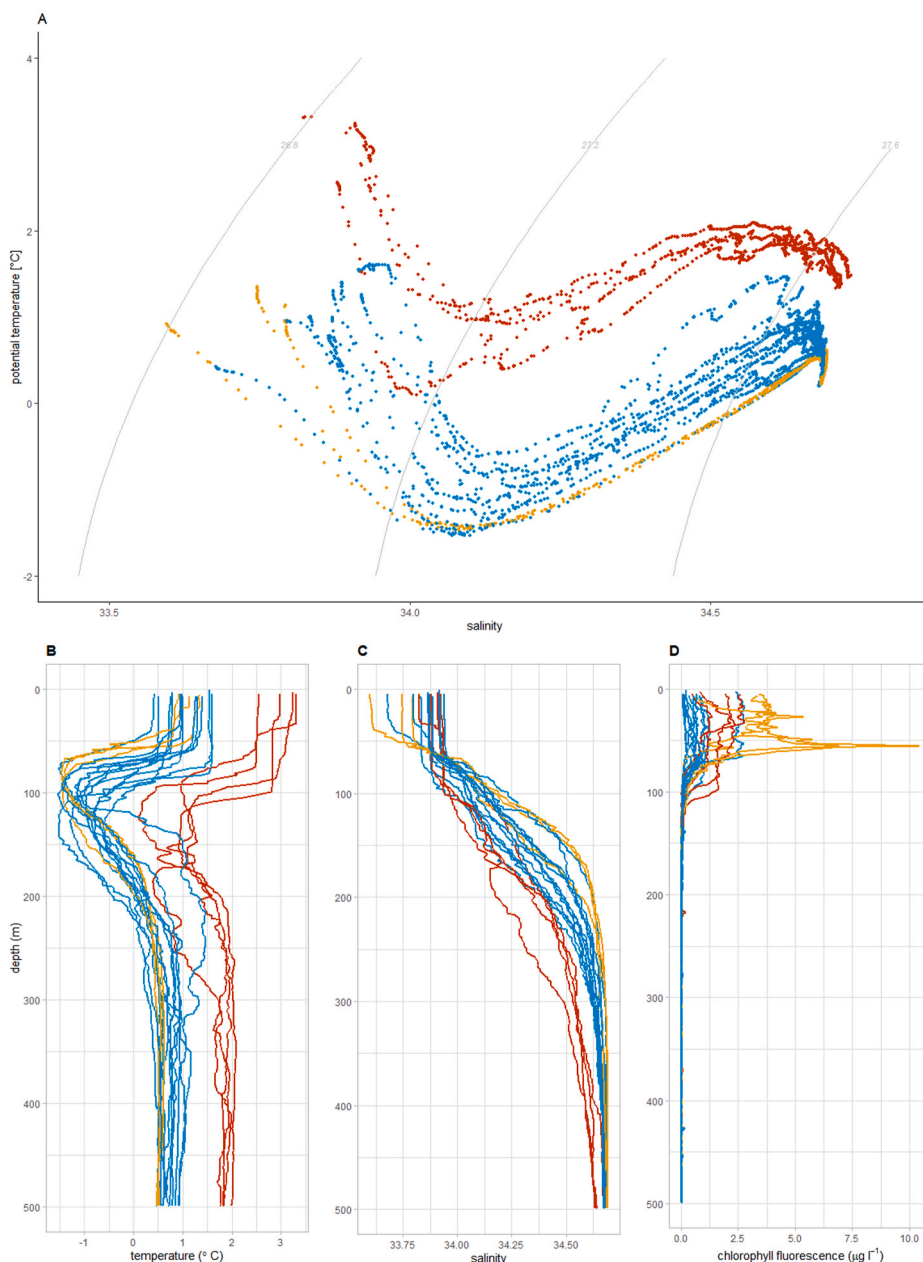

Fig. 3. A: Potential temperature-salinity profiles from CTDs deployed at all stations. Colours represent the two principal water masses which correspond to north (red) and south (blue + orange) of the Southern Boundary (SB), respectively. Orange represents a sub-group of stations with distinct fluorescence properties. Isopycnals of potential density are shown. B–D: profiles of B) potential temperature (°C), C) salinity, and D) chlorophyll fluorescence (μg l^{-1}) from 0 to 500 m taken from CTD deployments made at each station. Colours, as for A, represent water mass and fluorescence properties: red = stations north of the SB, corresponding to red in A; orange = stations to the east of the islands with high chlorophyll fluorescence (stations 5, 13 and 14 in Fig. 1); blue = all remaining stations south of the SB.

all the CTD station data showed that stations fell broadly into two water mass zones (Fig. 3A), with some mixing between them. These water mass zones correspond broadly to the cold waters south of the SB (blue and orange profiles), and the relatively warmer waters of the ACC (red profiles) to the north. Salinity averaged over the mixed layer (ML) ranged from 33.6 (station 5 on the south-eastern edge) to 33.9 (station 12) and was lowest along a band running north from the far south, along the eastern edge of the archipelago (Fig. 4B).

Mixed layer depth (MLD) varied from 33 m to 101 m (mean 65 ± 18 m) and showed no correlation with mixed layer temperature. There was no significant relationship between MLD and any measure of chl-a. Chl-a at the chl-maximum ranged from 0.25 to 10.44 µg l^{-1} (Fig. 4C). Many stations displayed a clear subsurface fluorescence maximum (SFM), the depth of which varied between 17 m and 78 m, and which was evident in both fluorescence profiles (Fig. 3D) and extracted pigment samples (Supplementary Fig. 1). Mean chl-a over the ML, derived from the CTD, was well correlated with surface chl-a ($R^2 = 0.78$, p < 0.0001) with one outlier corresponding with the SFM at station 14. Integrated chl-a over the ML derived from CTD fluorescence ranged from 4.06 to 169.43 µg l^{-1} and phaeophytin-a over the ML ranged from 2.92 to 178.33 µg l^{-1} (Supplementary Fig. 1). Due to strong collinearity between all measures of in-situ chlorophyll (CTD and extracted filters), only integrated CTD fluorescence (converted to chl-a) was retained for subsequent statistical analyses.

3.3. Phytoplankton community

3.3.1. Composition

Overall, phytoplankton abundances were similar at both 5 m and the chl-max throughout the survey region, ranging from $<1.5 \times 10^5$ to $\sim2.0 \times 10^6$ cells L^{-1} at 5 m and $<1.4 \times 10^5$ to 2.3×10^6 cells L^{-1} at the chl-max (Table 1). Proportions of taxonomic groups were also similar at both depths: flagellates dominated, ranging from $\sim5.3 \times 10^4$ to 1.7×10^6 cells L^{-1} and 20–88% in each sample. Diatoms were the next most abundant, ranging from 1.7×10^4 to 6.0×10^5 cells L^{-1} and 7–71% in each sample. There was a strong inverse correlation ($R^2 = 0.91$, p < 0.0001) between proportions of flagellates and diatoms, with diatoms comprising the majority at stations 8, 10, 13, 14 and 15 and flagellates dominating at the other stations.

Dinoflagellates were most abundant north of the SB and along the eastern edge of the SSI, reaching maximum abundances of $>7.30 \times 10^4$ cells L^{-1} in the chl-max at station 5, and up to 9% total contribution (chl-max at station 10). *Phaeocystis antarctica* was present in <60% samples but only contributed a substantial proportion (3–15%) in the chl-max at stations 3, 4 and 15. Foraminifera and Acantharia were present in low abundances at a small number of stations.

3.3.2. Community structure

Multivariate analysis of phytoplankton data identified 4 significant clusters (Table 2, Fig. 5) which broadly corresponded to east of the SSI
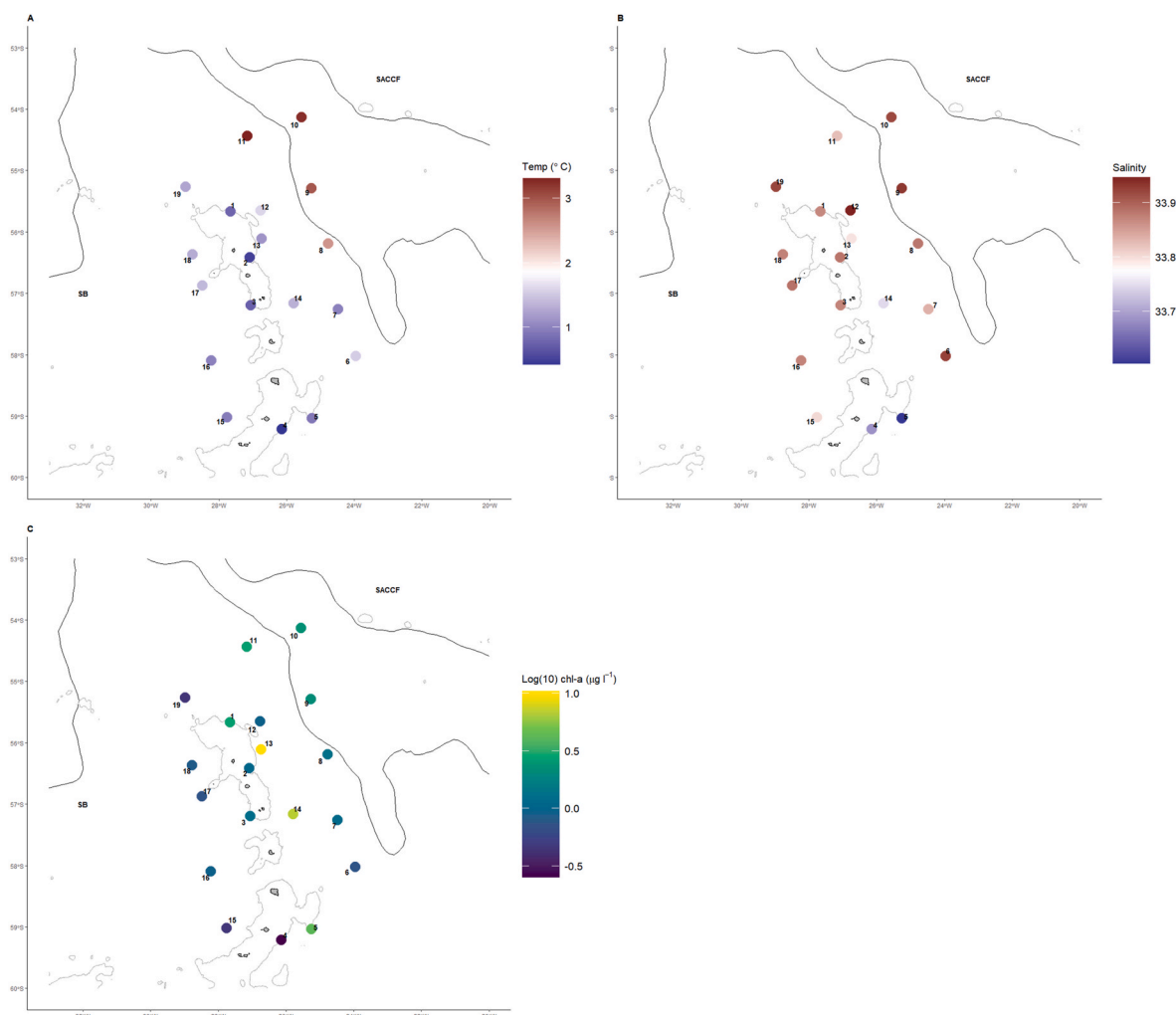

Fig. 4. Maps of A) sea surface temperature (SST °C), B) salinity over the mixed layer, and C) log chlorophyll-a (µg l^{-1}) at the chlorophyll maximum, obtained by the CTD are shown for each station sampled. Frontal positions are taken from Park and Durand (2019). The grey lines indicate the position of the 2000 m isobath.

Table 2
Average abundances (cells L^{-1}) and average carbon biomass (pg C) of main phytoplankton groups to each station cluster (left hand columns) and the % contribution of each group to the total for each cluster (A-D). Percentages may not total 100% due to rounding. Totals refer to the average total abundance or biomass of cells at the chl-max for each station cluster.

|	Metric	A (east)		B (west)		C (nSB)		D (periphery)		Total
Diatoms	abundance	356,726	31%	137,043	14%	376,155	57%	63,271	32%	2,549,970
	biomass	442,029,163	96%	73,253,696	80%	298,122,575	91%	35,890	85%	2,432,237,231
Dinoflagellates	abundance	47,340	4%	21,857	2%	37,184	6%	4285	2%	303,387
	biomass	13,401,588	3%	13,558,769	15%	27,037,656	8%	152,916	13%	180,791,373
Phaeocystis	abundance	7351	1%	51,458	5%	700	0%	4084	2%	198,249
	biomass	24,479	0%	171,356	0%	2331	0%	158,562	0%	660,169
Planktonic ciliates	abundance	4284	0%	2808	0%	740	0%	3180	2%	38,657
	biomass	272,273	0%	58,975	0%	35,010	0%	71,118	0%	1,498,763
Silicoflagellates (Dictyocha)	abundance	3387	0%	2116	0%	2246	0%	3772	2%	39,861
	biomass	176,100	0%	110,053	0%	116,802	0%	180,076	0%	2,072,769
Flagellates	abundance	723,685	63%	752,916	78%	243,815	37%	119,906	60%	5,516,962
	biomass	4,550,013	1%	4,733,796	5%	1,532,933	0%	753,885	1%	34,686,717
TOTAL	abundance	1,143,330	100%	968,199	100%	660,940	100%	198,522	100%	8,649,080
	biomass	460,453,616	100%	91,886,645	100%	326,847,308	100%	68,246,324	100%	2,651,947,021
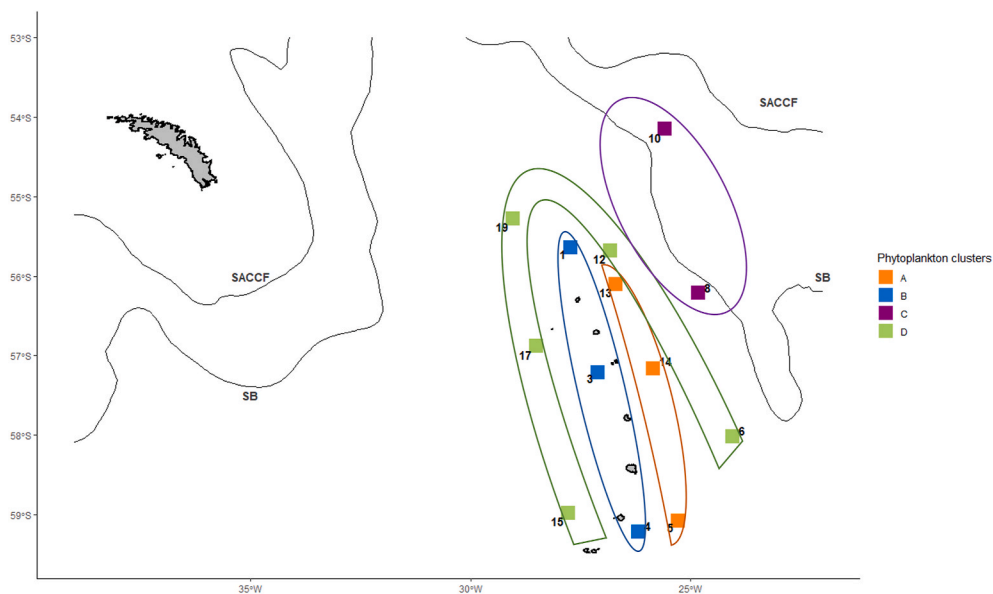
Fig. 5. Distribution of station clusters (group average clustering) based on phytoplankton community structure at the chlorophyll maximum.

(A), west of the SSI (B), north of the SB (C), and stations on the periphery of the archipelago (D). SIMPER analysis (Supplementary Table 2) showed that stations in cluster A had significantly greater proportions of large diatoms such as *Rhizosolenia* spp. and *Proboscia* spp., and many small centric diatoms and dinoflagellates. *Phaeocystis antarctica* and

Corethron spp. were substantially more abundant in group B, and in group C diatoms of the genera *Thalassionema* spp., *Pseudo-nitzschia* spp., *Fragilariopsis* spp. and *Chaetoceros* spp. were most abundant. Group D stations differed most in their much lower abundances of most taxonomic groups. Whilst diatoms were on average more abundant in group
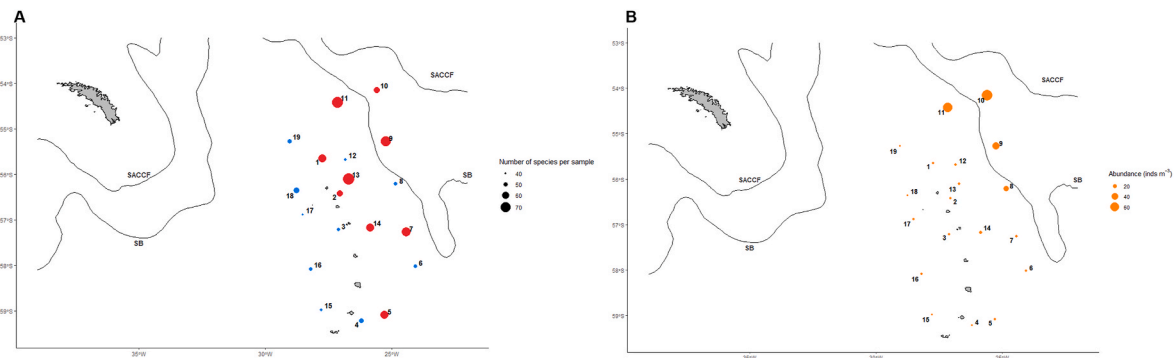

Fig. 6. Maps showing A) the number of taxa per sample for stations around the South Sandwich Islands, with colours representing stations where diversity was above (red) or below (blue) the median (55 taxa); B) the zooplankton abundance (individuals m^{-3}) for stations around the South Sandwich Islands. For both maps, values are indicated by the size of the bubble. Data include mesozooplankton, macrozooplankton and nekton.

C north of the SB, they were mostly small. Group A also had high abundances of small diatoms (not significantly different to Group C), but in addition, groups A and B both had substantially higher numbers of large diatoms present (Supplementary Fig. 2).

3.4. Zooplankton community

3.4.1. Composition

In total, 160 taxa were identified, 107 of which were found in RMT1 nets (nominally mesozooplankton) and 72 in RMT8 nets (nominally macrozooplankton/nekton). Abundances ranged from <1 individual m^{-3} to >73 inds m^{-3} (Table 1, Fig. 6B). Number of species per sample ranged from 40 to 76 (median 55) and increased from west to east (Fig. 6A), with all stations on the western side of the archipelago below the median. There was also a diurnal component with generally lower numbers of species at stations sampled during the day (Table 1).

Biomass (mg m^{-3}) ranged from 1.9 mg m^{-3} to 26.0 mg m^{-3} (median 8.2 mg m^{-3}; Table 1). Total biomass was dominated by the macrozooplankton/nekton but this varied with station: macrozooplankton/nekton comprised between 23 and 93% of total biomass (mean 72%); and mesozooplankton between 7 and 77% (mean 28%) of total biomass. There was a strong diurnal influence, with significantly higher biomass found at night-time stations (mean 17.0 ± 5.6 mg m^{-3}) compared to those sampled during the day (mean 6.9 ± 3.4 mg m^{-3}). This was driven by the effect of vertically migrating macrozooplankton/nekton, principally euphausiids and myctophids (Table 3B).

Calanoid copepods dominated the mesozooplankton biomass (>55% with 55 unique taxa identified), followed by euphausiids (32%),

polychaetes (6%), amphipods (3%), siphonophores (3%) and copepod nauplii (1%) (Fig. 8, Supplementary Table 3). Within this, five species (*Rhincalanus gigas*, *Calanoides acutus*, *Calanus propinquus*, *C. simillimus* and *Metridia gerlachei*) accounted for >70% of the copepods; *Thysanoessa* spp. was the dominant euphausiid (38% of euphausiid biomass) and the larval stages of euphausiids (nauplii, calyptopis and furcilia) comprised 9% of total euphausiid biomass (Table 3A).

Macrozooplankton/nekton was dominated by euphausiids (32%), followed by siphonophores (24%), myctophid fish (16%) and salps (7%) (Fig. 8, Supplementary Table 3). *Thysanoessa* spp. was the dominant euphausiid, contributing 70% to the total, with *Euphausia superba*, *E. triacantha* and *E. frigida* contributing 18%, 6% and 4% respectively. Within the myctophids, >87% were comprised of *Gymnoscopelus braueri* and *Electrona antarctica* (Table 3B). See Supplementary Fig. 3 for maps showing the distribution of key taxa.

3.4.2. Mesozooplankton community structure

Cluster analysis revealed that stations formed three clear groups corresponding spatially to stations to the north of the Southern Boundary (nSB, Group C), the majority of stations south of the SB (sSB, Group B) and stations 4 and 15 that we term 'far south' (Group A; Fig. 7 and Supplementary Fig. 4, top panel). Dissimilarities between the groups based on SIMPER analysis ranged from 57.2 to 77.7% dissimilarity (Supplementary Table 4). Group A (far south) differed from Groups B and C principally in lower biomasses of all taxa, particularly calanoid copepods such as *R. gigas*, *Calanoides acutus*, *Calanus simillimus* and *C. propinquus*; larval euphausiids; and polychaetes; as well as a near absence of the euphausiid *Thysanoessa* spp. Group B (nSB) was

Table 3

Average biomass (mg m^{-3}) of the dominant taxa per cluster group (where groups correspond to those in Fig. 7); the % contribution of each taxon to the total biomass; and the % contribution of each taxon to the biomass of its higher taxonomic group for A) mesozooplankton and B) macrozooplankton and nekton (night-time stations only).

A) Mesozooplankton taxon	A (far south)	B (nSB)	C (sSB)	% contribution to total	% contribution to taxonomic group	Taxonomic group
Hyperiid amphipods	0.04	0.03	0.10	2.4	81.8	Amphipoda
Themisto gaudichaudii	0.00	0.06	0.00	0.5	16.6	Amphipoda
Rhincalanus gigas	0.01	2.84	0.21	23.6	42.9	Calanoida
Calanoides acutus	0.04	0.35	0.39	11.1	20.0	Calanoida
unidentified calanoid copepods*	0.02	1.11	0.06	8.8	16.0	Calanoida
Euchaetidae	0.03	0.19	0.06	2.6	4.8	Calanoida
Calanus propinquus	0.00	0.15	0.02	1.5	2.7	Calanoida
Metridia gerlachei	0.00	0.08	0.04	1.4	2.6	Calanoida
Calanus simillimus	0.00	0.16	0.00	1.1	1.9	Calanoida
Paraeuchaeta	0.00	0.03	0.02	0.8	1.5	Calanoida
Euchirella	0.00	0.11	0.00	0.8	1.4	Calanoida
Metridia lucens	0.00	0.09	0.00	0.6	1.2	Calanoida
unidentified Euphausiacea	0.00	0.00	0.03	13.5	42.0	Euphausiacea
Thysanoessa	0.00	0.11	0.37	12.2	37.8	Euphausiacea
larval euphausiids**	0.01	0.39	0.01	3	9.0	Euphausiacea
Euphausia frigida	0.00	0.08	0.10	2.7	8.5	Euphausiacea
Euphausia triacantha	0.00	0.01	0.01	0.2	0.6	Euphausiacea
Euphausia superba	0.00	0.00	0.00	0.01	0.2	Euphausiacea
Polychaeta	0.01	0.28	0.16	5.4	97.1	Polychaeta
Siphonophora	0.02	0.04	0.10	2.5	100.0	Siphonophora

B) Macrozooplankton & nekton taxon	A (west)	B (stn. 79)	C (nSB)	D (east)	% contribution to total	% contribution to group	Group
Thysanoessa	0.42	9.52	2.07	0.57	18.9	70	Euphausiacea
Euphausia superba	1.40	0.59	0.03	0.66	4.7	17.5	Euphausiacea
Euphausia triacantha	0.12	0.55	0.69	0.03	1.5	5.5	Euphausiacea
unidentified euphausiids	0.32	0.00	0.24	0.28	1.2	4.4	Euphausiacea
Euphausia frigida	0.07	0.09	0.25	0.09	0.7	2.6	Euphausiacea
Gymnoscopelus braueri	0.63	0.87	1.94	1.60	10	61.2	Myctophidae
Electrona antarctica	0.18	0.42	0.81	0.85	4.3	26.2	Myctophidae
Gymnoscopelus nicholsi	0.00	0.00	0.00	0.28	0.6	3.4	Myctophidae
Electrona carlsbergi	0.00	0.00	0.42	0.00	0.5	3.3	Myctophidae
Salpa thompsonii	0.00	1.25	0.14	2.42	6.3	90.9	Salpida
other unidentified salps	0.01	0.00	0.00	0.00	0.6	9.1	Salpida
Siphonophora	2.39	0.10	0.00	3.78	14.5	60.3	Siphonophora
Diphyes spp.	0.56	0.71	0.14	1.61	8.5	35.4	Siphonophora

* includes all developmental stages.

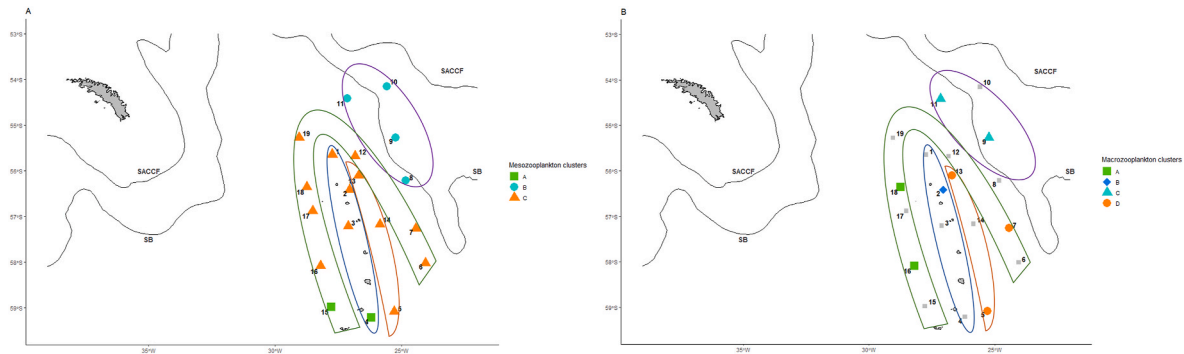* includes nauplii, calyptopis and furcilia stages.

Fig. 7. Map illustrating the spatial distribution of station clusters based on A) mesozooplankton species biomass and B) night-time macrozooplankton and nekton species biomass. For macrozooplankton and nekton, day-time stations are shaded grey for clarity but are excluded from the clustering as they showed no discernible structure. Overlain on both plots are the positions of the phytoplankton clusters (A, east = orange, B, west = blue, C, nSB = purple, D, peripheral = green; see Fig. 5).
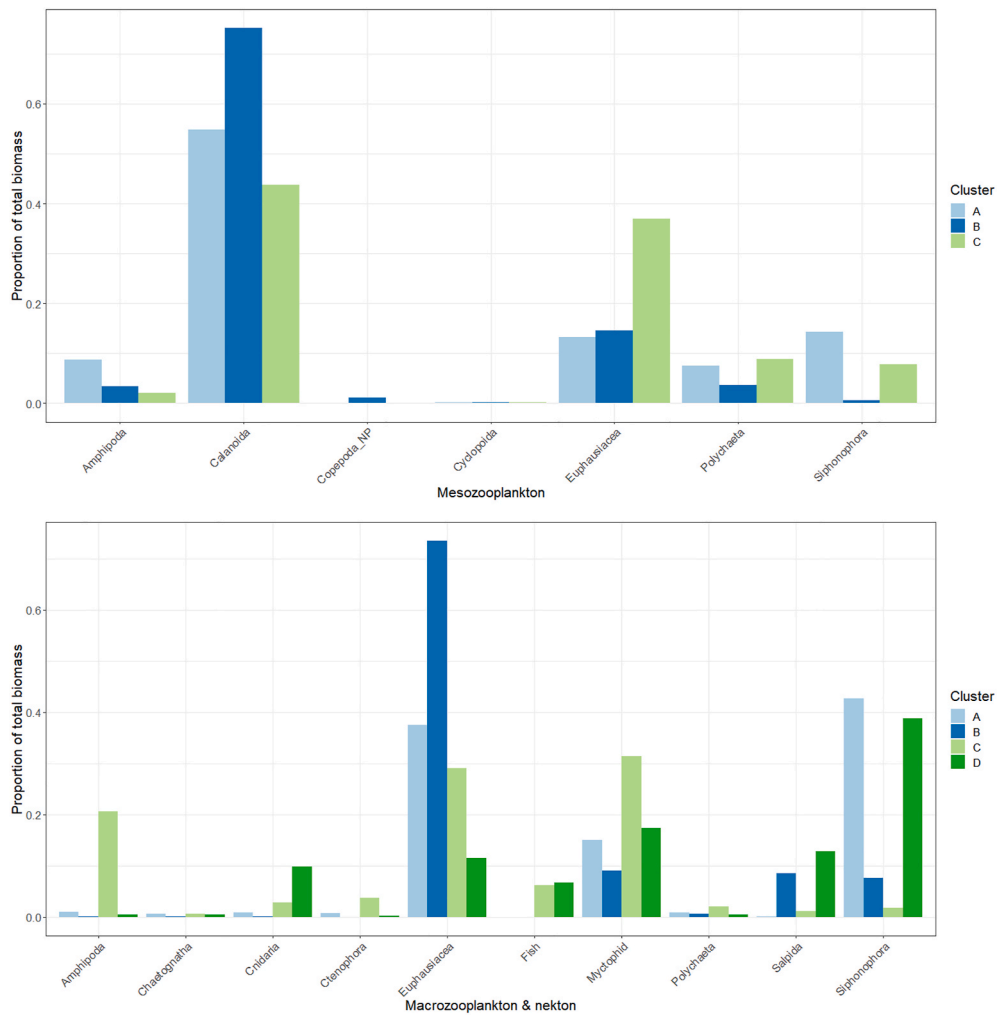

Fig. 8. Average proportion (%) of main taxonomic groups to total station biomass by cluster group for A) mesozooplankton and B) macrozooplankton and nekton. For macrozooplankton and nekton, cluster groups only include night-time stations.

differentiated from the other groups by having significantly higher biomasses of calanoid copepods, particularly *R. gigas*, *C. simillimus* and *C. propinquus* and relatively high biomass of larval euphausiids, the latter of which were almost entirely absent in Group C (sSB). The copepod *C. simillimus* was a strong contributor to biomass in Group B but entirely absent in Groups A and C. Group C on the other hand had much higher biomasses of euphausiids, particularly *Thysanoessa* spp. but a near absence of larval euphausiid stages. Biomass of *C. acutus* was

highest in Group C although this was most marked in comparison to Group A.

3.4.3. Macrozooplankton/nekton community structure

A significant difference between daytime and night-time biomass was found for macrozooplankton/nekton (ANOSIM, p = 0.01), which was not apparent in mesozooplankton (ANOSIM, p = 0.1). These data were therefore split and analysed as daytime and night-time subsets.

Daytime samples had no apparent structure, with all stations except for station 4 forming one single cluster. Station 4 was characterised more by polychaetes, chaetognaths, gelatinous taxa such as siphonophores and the highest and second highest biomasses of the pteropods *Clione lima-cina antarctica* and *Clio pyramidata*, respectively. Night-time stations formed three main groups: Group A on the western side of the archipelago, Group C containing stations north of the SB, and Group D on the eastern side; along with Group B which comprised station 2 alone (Supplementary Fig. 4, bottom panel).

Group A was distinguished by lower biomasses of macrozooplankton/nekton compared to other groups (mean 6.6 mg m^{-3} vs 14.3 mg m^{-3} for the other night-time stations), an absence of *Salpa thompsoni*, relatively higher biomasses of siphonophores, and the highest *E. superba* biomass overall (2.7 mg m^{-3} at station 18) (Supplementary Table 5). Group C (nSB) was distinct in having much higher biomass of *Themisto gaudichaudii* than all groups, very low *E. superba*, comparatively higher *E. triacantha* biomass, and a complete absence of siphonophores. Group D was differentiated largely by having a higher biomass of *S. thompsoni* than all other groups, and more of the mesopelagic fish *E. antarctica*, *G. braueri* and *Bathylagus* spp. than groups A and B. Group B differed from other groups most clearly in the extremely high biomass of *Thysanoessa* spp. compared to any other group, and more *S. thompsoni* than all but Group D (to which it was comparable).

3.5. Environmental correlates of zooplankton

BIOENV identified SST to be the best single variable explaining the structure of the mesozooplankton over the top 200 m (corr = 0.518, p = 0.01, Supplementary Table 6). However, the inclusion of additional variables improved the model fit. The best explanatory model was produced with four variables: SST, in-situ integrated chl-a, distance to the ice-edge and water mass zone (corr = 0.650, p = 0.01). For macrozooplankton/nekton, the BIOENV analysis was run on the night-time stations only. The best single variable explaining the structure of macrozooplankton/nekton in the top 200 m during night was distance to the ice-edge (corr = 0.534, p = 0.01). Again, model fits improved with additional variables, and the best model included three variables: distance to the ice-edge; satellite chlorophyll for the month prior to the study period; and distance to the shelf-break (corr = 0.798, p = 0.01).

3.6. Spatial congruence between phytoplankton and zooplankton community structure

To examine any spatial congruence between phytoplankton, mesozooplankton and macrozooplankton/nekton community structure, we overlaid the phytoplankton cluster map (Fig. 5) onto the meso- and macrozooplankton/nekton station clusters (Fig. 7). The region where all three groups showed greatest congruence was north of the SB, where there was a distinct cluster in each of the three groups. Congruence between the three groups was less evident south of the SB. There, mesozooplankton formed one large cluster (cluster C, Fig. 7A) and a second small one (cluster A, Fig. 7A) which straddled phytoplankton clusters B and D (Fig. 5). Spatial congruence was not particularly evident between macrozooplankton/nekton and mesozooplankton, but it was more apparent between macrozooplankton/nekton and phytoplankton. In particular, macrozooplankton/nekton cluster D (Fig. 7B) encompassed stations on the eastern edge of the archipelago and overlapped with the phytoplankton eastern cluster A (Fig. 5). Similarly, macrozooplankton/nekton clusters A and B (Fig. 7B) showed elements of congruence with the phytoplankton peripheral cluster D, and western cluster B (Fig. 5) although it must be noted that there was only one macrozooplankton/nekton station in cluster B. The relationship between the two was not so strong at the eastern edge of the archipelago.

4. Discussion

Across the South Sandwich Island (SSI) region, we found distinct community plankton structure at the mesoscale level, with four spatially delimited groups of phytoplankton and macrozooplankton/nekton taxa, and three groups of mesozooplankton taxa. These groups were characterised by a relatively small number of dominant taxa that varied predominantly in their relative abundances or biomasses, although a small number of taxa were confined to one group alone. This structure was strongly related to environmental conditions, particularly to sea surface temperature, surface chlorophyll-a and sea-ice. There was some spatial congruence between phytoplankton and the two zooplankton groups, particularly with regards to the influence of the Southern Boundary of the ACC (SB) on respective community structure.

4.1. SSI phytoplankton bloom development

Our study took place during austral summer 2019, when the sea-ice had retreated far south of 60 °S and the islands were in open water. Two principal water mass zones were detected, reflected by their θ-S properties. These corresponded to distinct surface water mass properties, with generally warmer and more saline waters north of the SB and colder and more variable salinity south of the SB. Differences in the subsurface water masses were also evident with both the temperature minimum and temperature maximum layers colder and generally more saline south of the SB. Based on the locations of these stations, the SB seemed to be positioned slightly further south than the mean position of Park and Durand (2019), as also suggested from climatological data (Thorpe and Murphy, this issue).

At the time of our study (late January-early February), a phytoplankton bloom had developed along the eastern edge of the archipelago, with extremely high (up to >10 μg l^{-1}) subsurface fluorescence values. Integrated chl-a over the mixed layer depth (MLD) averaged 142 ± 10 μg l^{-1} over the three stations located along this eastern band (5, 13 and 14) and were the highest chl-a values observed across the region. Satellite imagery from the two months prior to our study indicate that bloom onset occurred at the south-eastern edge of the archipelago in November, with the bloom propagating northwards, along the eastern edge, over a period of approximately 2.5 months and limited to the east by mesoscale features related to the SB.

The bloom is evident within the group of stations south of the SB as a sub-group of stations with very high chl-a concentration, which coincided with significantly lower salinities within the mixed layer. Sea-ice retreat is one possible explanation for both lower salinity and elevated chl-a. However, during the previous winter, sea-ice covered almost the entire archipelago, and since nearby stations on the western side did not share this characteristic of elevated chl-a, we suggest that this is unlikely to be due to ice-edge retreat alone but to a combination of factors, including local water column properties and nutrient availability. In a previous study, Perissinotto et al. (1992) hypothesised that bloom formation was due to the stabilisation of the water column as a result of glacial run-off, resulting in the coincidence of lower salinities, shallower MLDs and elevated chl-a across the SSI shelf. However, their study did not incorporate the eastern side of the archipelago. It is likely that nutrient input from both the iron-enriched waters originating upstream of the SSI and local interaction with the complex bathymetry of the SSI arc, in connection with the timing of the sea ice retreat, is an important driver of phytoplankton blooms around the SSI (e.g. Jiang et al., 2019; Thorpe and Murphy, this issue; Tynan et al., 2016).

The Southern Ocean (SO) is the largest high nutrient, low chlorophyll (HNLC) oceanic province, and iron is a key limiting micronutrient (de Baar et al., 1995; Martin, 1990). Interactions between oceanography and bathymetry that generate iron inputs are responsible for large and persistent phytoplankton blooms in other parts of the SO, including around South Georgia, the Crozet Plateau and the Kerguelen Islands (e.g. Bakker et al., 2007; Korb et al., 2005; Poulton et al., 2007). However,

whilst blooms tend to occur downstream of these other island groups as a result of the interaction between the prevailing current and shoaling bathymetry (the 'island mass effect'), it is not clear that the same is true of the SSI. Whilst the SB is constrained along the eastern bathymetry of the South Sandwich Islands arc, bloom formation and magnitude are variable both in time and space (Thorpe and Murphy, this issue). The bloom observed during our survey appeared to propagate northwards, suggesting that bloom dynamics around the SSI may be more complex than in other regions. Furthermore, in addition to iron, it has been suggested that manganese co-limits the growth of phytoplankton, with volcanic events a potential source for the relief of both iron and manganese limitation (Achterberg et al., 2013; Browning et al., 2014). The SSI is an active tectonic region and an eruption on Saunders Island was ongoing during the study period. Whilst we were unable to test it directly, it is possible that the bloom was enhanced not only by the input of micronutrients of lithogenic origin but also those of a volcanic origin.

4.2. Phytoplankton community structure

In terms of phytoplankton structure, stations clustered into four geographically defined groups, corresponding to north of the Southern Boundary (nSB, Group C), east of the archipelago (Group A), west of the archipelago (Group B), and stations around the periphery of the islands (Group D). Excluding flagellates, diatoms were the dominant group in all station groupings, although they contributed substantially less to group B where *Phaeocystis antarctica* comprised a greater proportion of the phytoplankton. Where diatoms dominated, composition varied considerably between groups. Both Groups C (nSB) and D (periphery) were dominated by the weakly silicified diatom *Chaetoceros* spp. which is considered typical of naturally iron-fertilised regions (Korb et al., 2005, 2012; Lasbleiz et al., 2016) and has been experimentally shown to be limited by iron (e.g. Pausch et al., 2019; Petrou et al., 2014). However, within Group D stations, both total abundance and diatom abundance was significantly lower, and, relative to diatoms, there were greater proportions of both flagellates and *Phaeocystis antarctica*, which can be suggestive of lower productivity and lower export waters. In Group C stations, higher chl-a maximum concentrations (2.18 µg l^{-1}) were mirrored by greater phytoplankton species richness and abundance, and the diatom community comprised moderate abundances of *Fragilariopsis* spp., *Nitzschia/Pseudonitzschia* spp. and *Thalassionema* spp. (ranging from >21,000 cells l^{-1} to >74,000 cells l^{-1} respectively), along with the larger *Guinardia* spp. which was only found in substantial numbers in this group. Stations in this group were situated at the northern end of the South Sandwich Trench in deep water, so iron input due to interaction with SSI bathymetry seems unlikely. Satellite chl-a was also elevated, and appeared connected by the SACCF to the bloom region around South Georgia, thus potentially seeding the bloom north of the SSI (Whitehouse et al., 2008).

The eastern group on the other hand was dominated by the small, weakly silicified diatom *Thalassiosira* spp. that also responds to iron-enrichment and dominates blooms around the Kerguelen Islands (Lasbleiz et al., 2016) and South Georgia (Korb et al., 2012). In an earlier investigation of waters south of the SB and overlying the South Scotia Ridge, *Thalassiosira* spp. also dominated and was coincident with elevated chl-a (Korb et al., 2005), putatively a response to increased light availability and iron enrichment following ice-edge retreat. Due to its rapid build-up and aggregation of biomass, blooms of *Thalassiosira* spp. can be responsible for the export of large amounts of carbon (Korb et al., 2012). This group also had much higher proportions of large diatoms, particularly the large and heavily silicified *Rhizosolenia* spp. and *Proboscia* spp. which, whilst not specific to the SO, are commonly found in the waters of the Weddell Sea (Scott and Marchant, 2005) and in SO sea-floor sediments (Armand and Zielinski, 2001), and have been implicated in the upward transport of nitrate from depth (Singler and Villareal, 2005; Villareal et al., 2014).

In contrast, the western side of the archipelago was characterised by

greater abundances of *Phaeocystis antarctica*. This is a common SO species and can form blooms in its own right (Tagliabue and Arrigo, 2003), and the greater light sensitivity of *Phaeocystis* spp. can allow it to exploit low irradiances at the start of austral spring, often leading to early blooms during spring and a temporal succession to diatoms (Nissen and Vogt, 2021). However, *Phaeocystis* spp. can also be an indicator of transition to later stages, or decline, of the bloom (Poulton et al., 2007). Satellite imagery does not suggest the presence of bloom conditions on the western side of the islands in the months prior to our study. However, these data only represent surface conditions and we observed subsurface fluorescence maxima (SFMs) which are common across the SO (Baldry et al., 2020), with values far in excess of satellite-estimated surface values. Relying on satellite imagery alone may therefore not capture the full magnitude of bloom dynamics (Whitehouse et al., 2008). A better understanding of the processes controlling productivity and bloom dynamics is therefore essential, both in order to understand the spatial variability of phytoplankton and how this is linked to variables such as ice-retreat, bathymetry and hydrography, as well as potential implications for nutrient cycling.

4.3. Zooplankton and nekton community structure

A preliminary analysis of the combined (RMT1 + RMT8) datasets showed that stations clustered strongly on the basis of whether they were taken during day or night and that this was almost entirely driven by a small number of macrozooplankton/nekton taxa. The most dominant of these were euphausiids, specifically *Euphausia triacantha*, *E. frigida* and *E. superba*; mesopelagic fish, particularly *Gymnoscopelus braueri* and *Electrona antarctica*; and the salp, *Salpa thompsoni*. These species are known to carry out extensive DVMs and to have deep vertical distributions during both day and night (Lancraft et al., 1989; Liszka et al., 2021; Piatkowski, 1985; Piatkowski et al., 1994) or to be able to avoid net capture in the upper 200 m during daylight (e.g. Collins et al., 2012); thus, over the 200 m depth of our sampling range, we probably did not capture the full geographical distribution of these organisms around the SSI. Splitting the macrozooplankton/nekton analysis by day and night showed that, during daytime, the top 200 m showed no discernible structure and was relatively homogeneous across the whole area, with biomass dominated by *Thysanoessa* spp., *Themisto gaudichaudii* and siphonophores. Night-time stations however revealed more spatial structure, which we attribute largely to the migration of many of these biomass dominant taxa into (or out of) the upper 200 m. Three main groups plus one single station emerged, which broadly corresponded to stations north of the SB, stations on the eastern edge of the archipelago and stations on the west.

No such day-night structure was found in the mesozooplankton, and although there was some evidence of DVM by a few taxa (e.g., copepods *Calanus simillimus*, *Gaetanus* spp., *Metridia* spp. and *Scolecithricella* spp.; and euphausiids *E. triacantha* and *Thysanoessa* spp.), no significant diurnal shifts occurred to bias the analysis or obscure the clear spatial structure. Larger species tend to have deeper migratory amplitudes than smaller species (Atkinson et al., 1992b; Ward et al., 1995), and the bulk DVM movement for key copepod taxa e.g., *C. acutus*, *C. simillimus* and *C. propinquus* is often observed within the top 200 m (Atkinson et al., 1992a). Thus our 200 m integrated net hauls effectively circumvented any potential day-night bias and accurately reflected the mesozooplankton distribution across the SSI. In terms of structure in the mesozooplankton community, stations formed three clusters which corresponded to those north of the SB, two stations at the far south of the archipelago, and the remainder of stations south of the SB and encompassing the main archipelago.

For both meso- and macrozooplankton/nekton, there was a clear difference in community between the waters north (nSB) and south (sSB) of the SB. As for other parts of the SO, differences between groups were often defined by relatively small numbers of common taxa. nSB macrozooplankton/nekton was dominated by myctophids (principally

G. braueri, E. antarctica and *E. carlsbergi*), euphausiids, and the amphipod, *Themisto gaudichaudii*. Although *Thysanoessa* spp. dominated the euphausiids, biomass was lower here in comparison to that in the sSB, whereas the highest biomass of the more sub-Antarctic euphausiid, *E. triacantha*, occurred in this group. This is consistent with what appears to be a warmer water community, with the mesozooplankton community composition also demonstrating a greater degree of similarity to the waters around South Georgia, in the northern part of the Scotia Sea. Here, calanoid copepods were the overwhelmingly dominant group, comprising >75% of the mesozooplankton biomass, with the sub-Antarctic *R. gigas* the greatest contributor and *C. simillimus* only found in this northern group (Atkinson, 1991).

sSB mesozooplankton biomass was generally more evenly distributed between calanoid copepods (44%) and euphausiids (37%). The composition was more indicative of a colder water community, with *R. gigas* and *C. simillimus* much reduced or absent respectively, and instead the highest biomass of *C. acutus*. In terms of euphausiids, *Thysanoessa* spp. dominated, and the highest biomass of *E. frigida* also occurred in this group. Wallis et al. (2020) found *C. acutus* to be a key determinant of the abundance of *T. macrura* in the southern Kerguelen region, where they are thought to be a major food resource for higher predators around the region. Associations in the timing of lipid accumulation and composition between *T. macrura* and *C. acutus* also lend support to the idea that *C. acutus* are a major prey item for *T. macrura* (Atkinson, 1998; Hagen and Kattner, 1998; Wallis et al., 2020). A number of taxa (for example *Aetididae, C. propinquus, Ctenocalanus* spp., *Oithona* spp., *Oncaea* spp., *Scolecithricella minor*, and fish larvae) were observed in relatively higher abundances at the stations on the eastern edge of the archipelago (corresponding to the position of the bloom), but either these differences were not sufficiently strong, or sufficiently distinct, to be reflected in the overall structure. On the other hand, a difference in community composition between east and west of the archipelago was apparent in the macrozooplankton/nekton structure. Stations on the eastern edge had a much higher occurrence of *S. thompsoni* (13% of total biomass) and myctophids, and the lowest biomass of euphausiids. This contrasted with the western side where siphonophores were the biggest contributor to the biomass, and euphausiids, particularly *E. superba*, were a relatively much greater contributor (>37% total biomass vs <12%). It is worth noting that, since the mesozooplankton was sampled with a 300 μm mesh net, some underestimation of biomass of the smaller copepods and their copepodite or nauplar stages is likely (Dubischar et al., 2002; Fransz and Gonzalez, 1997; Gallienne and Robins, 2001). For cyclopoids such as *Oithona* spp. and *Oncaea* spp., a mesh size of 100 μm is considered best practice (Fransz and Gonzalez, 1997), and Gallienne and Robins (2001) estimate that a 200 μm mesh WP2 net may underestimate biomass of this smaller fraction by one third. However, smaller mesh sizes also present greater risk of clogging and not quantitatively sampling the larger fraction. Since the same mesh size was used at all stations, we consider that the relative differences in composition between stations are consistent and do not change the overall patterns observed.

Within the macrozooplankton/nekton, myctophids were one of the three dominant groups. Many species such as *E. carlsbergi, G. fraseri, G. nicholsi, Protomyctophum tensioni* and *Krefftichthys anderssoni* were found in high abundances at only one or two stations, with no clear geographic or oceanographic association. On the other hand, *E. antarctica* and *G. braueri* were found to co-occur at all night-time stations, although abundances were greater on the eastern side of the archipelago, and to be absent from daytime nets, likely due to a combination of DVM and net avoidance (Collins et al., 2012). In the wider SO, myctophids are the most abundant mesopelagic fish and a key component of the SO food web, linking zooplankton and higher predators (Saunders et al., 2015a). Many have broad circumpolar distributions (Collins et al., 2012) and high genetic connectivity (Van de Putte et al., 2012). Both *E. antarctica* and *G. braueri* are also amongst the most abundant and ubiquitous myctophid species in the SO (Saunders et al.,

2014, 2015b) supporting the fact that they are found fairly abundantly across the SSI region. In terms of trophic linkages, myctophids are known to predate upon *Thysanoessa* spp., consuming ~12% of its daily production (Saunders et al., 2015a). *Thysanoessa* spp. was found ubiquitously throughout our survey area, in contrast to *E. superba* which had a lower and much more patchy distribution. *T. macrura* is a highly abundant SO euphausiid (Nordhausen, 1992), often comparable with, yet more widely dispersed than, the swarm-forming *E. superba*. Its wide thermal tolerance, short developmental period, and high dietary plasticity (Wallis et al., 2020), allow it to occupy a different ecological niche to *E. superba*, whilst its high lipid content (Hagen and Kattner, 1998) provides an energy-rich resource for higher predators such as penguins, birds and whales. We therefore suggest that the off-shelf SSI community provides a good example of a krill-independent trophic pathway (Murphy et al., 2007; Saunders et al., 2015a, 2019) and that *Thysanoessa* spp. and myctophids in this region are important conduits of energy between lower and higher trophic levels.

4.4. Drivers of structure and spatial congruence across plankton and nekton groups

There was some spatial congruence between phytoplankton, zooplankton and macrozooplankton/nekton clusters, but also some areas of spatial or trophic mismatch. The region with greatest congruence was nSB where, for all three faunal groups, communities formed one distinct cluster separated from the rest by the frontal boundary. Where environmental gradients are strong, differences between communities are often clearer, and greater similarity between trophic levels occupying the same niche may also be apparent (Karakassis et al., 2006). The SB intersected our study area, separating warmer and colder water mass zones and influencing the development of the bloom. SST explained the majority of the variance in mesozooplankton whilst distance to the ice-edge was a key response variable for both meso- and macrozooplankton/nekton. The latter was highly correlated to primary productivity (PP) for the month of December, indicating a link between past phytoplankton productivity and zooplankton community establishment, whilst the strong correlation between satellite-derived chl-a and PP also indicates that satellite-derived chl-a is a reasonable proxy for PP in the area. That both SST and surface chl-a north of the SB were more stable than to the south over the preceding two months may also help explain the observed spatial congruence between the three trophic levels, essentially smoothing out the effects that processes occurring at different temporal and spatial scales have on community turnover. Such patterns are consistent with previous studies of plankton ecology in the SO, with the mesozooplankton community around South Georgia known to be coincident with water mass zones (Ward et al., 2003), and to demonstrate close spatial association to phytoplankton community structure (Ward et al., 2005, 2007). Ward et al. (2003) demonstrated the close relationship between physics and biology when they found mesozooplankton community structure over four consecutive austral summers to be consistently associated with the different TS properties of the Sub-Antarctic Zone (SAZ), Polar Frontal Zone (PFZ) and Antarctic Zone (AAZ) respectively. Whilst some taxa such as *Oithona similis* and *Ctenocalanus* spp. were found in all water masses, *C. simillimus* and *Limicina helicina* were more typical in the PFZ, and *C. acutus* and *R. gigas* differentiated the more southerly waters of the AAZ. In the waters surrounding SG, the mesozooplankton has also shown a close association to phytoplankton, with stations forming similar spatial groupings corresponding broadly to shelf, western and eastern regions, and for this relationship to be largely driven by the size distribution of the phytoplankton rather than absolute phytoplankton biomass (Ward et al., 2005).

In contrast, congruence between the three faunal groups was less clear for the sSB stations and a degree of spatial and trophic mismatch was apparent. In particular, there was greater agreement between phytoplankton clusters and macrozooplankton/nekton clusters than

there was between mesozooplankton and either phytoplankton or macrozooplankton/nekton. Phytoplankton structure on the eastern edge of the archipelago indicated a clear response to the bloom, and this was mirrored to some degree by a similar cluster in the macrozooplankton/nekton. There was also some overlap between phytoplankton and macrozooplankton/nekton in groups on the western side of the archipelago, with a distinction between stations that were closer to the islands and those that were further off-shelf, which may reflect some overlap in their responses to environmental factors. Mesozooplankton on the other hand showed little spatial congruence with phytoplankton, with one primary cluster containing all but two of the stations. Turnover time is slower in mesozooplankton than phytoplankton, and the colder temperatures of the sSB mean that the mesozooplankton are more likely to be in earlier stages of development. Hence, a temporal mismatch may not be surprising. Alternatively, this mismatch may be the result of top-down control, with macrozooplankton or nekton predators exerting grazing pressure on the intermediate trophic level as it responds to elevated local productivity through their greater ability to migrate into such regions (McGinty et al., 2014). Nevertheless, direct evidence of such top-down control requires much greater resolution of predation rates, which are presently lacking.

4.5. Antarctic krill within the SSI plankton community

Historically, Antarctic krill (*Euphausia superba*) fishery catches at the SSI (CCAMLR Area 48.4) have been low or non-existent (CCAMLR, 2021), with the fishery preferring to focus efforts on Areas 48.1–48.3 (Western Antarctic Peninsula, South Orkneys and South Georgia). During the time of our survey, *E. superba* biomass was generally found to be low with a median biomass of 0.04 mg m^{-3} and reaching a maximum of 2.68 mg m^{-3} within our stratified nets. This is equivalent to a median of <0.01 g m^{-2} and a maximum of 0.54 g m^{-2} when integrated over the top 200 m sampling depth. The fisheries acoustic component of this survey estimated mean Antarctic krill biomass density to be 25.9 g m^{-2} (Krafft et al., 2021), using a swarms-based identification analysis. The swarming behaviour of Antarctic krill makes their distribution extremely patchy, and the detection and quantification of these swarms is best achieved by a mesoscale survey involving continuous monitoring (i.e. fisheries acoustics). The low probability of encountering an Antarctic krill swarm through the point sampling approach of nets makes this a non-ideal approach within the context of the spatial and temporal limitations of the present survey. In fact, no swarms of Antarctic krill were captured by our stratified net sampling campaign, making the mismatch between acoustic and net estimates of Antarctic krill biomass unsurprising. Indeed, in terms of other krill species, *Thysanoessa* spp. was the more dominant and ubiquitous euphausiid in this region during the time of our sampling (median 0.14 g m^{-2}, maximum 1.9 g m^{-2}). It is worth noting that in other parts of the Scotia Sea, Antarctic krill densities are often highest over shelf or shelf-break areas, and lower or more patchy in the open ocean (e.g. Atkinson et al., 2008; Murphy et al., 1997; Silk et al., 2016). Due to the steep shoaling of the SSI archipelago, the shallowest station sampled was >1000 m deep. Furthermore, with the exception of three stations, all our sampling locations were >50 km from the shelf-break. Therefore, the specific spatial design of the present net sampling study is unlikely to have sampled all potential habitats of Antarctic krill biomass in the vicinity of the SSI and thus underrepresented true levels of its biomass in this region.

4.6. Concluding remarks

This represents the first comprehensive description of the off-shelf plankton community structure across the South Sandwich Islands, and links between phytoplankton, zooplankton and nekton, and prevailing environmental conditions in this region. We find that the onset and development of a large phytoplankton bloom on the southern and eastern sides of the archipelago is related to physical variables, with sea-

ice retreat, hydrography and interaction with the bathymetry of the nearby islands all likely to be influential. The phytoplankton community structure is strongly related to oceanographic features, particularly the position of the SB of the ACC and bloom dynamics, with communities numerically dominated by diatoms, particularly on the eastern and northern sides of the archipelago, and a more heterogenous community with a greater contribution from *Phaeocystis* spp. on the western side. The mesozooplankton community is structured primarily on the basis of water mass properties, which differ to the north and south of the SB, but is also related to preceding primary productivity linked to sea-ice retreat, and in-situ chl-a. A warmer water community dominated by copepods characterised the group to the north of the SB, and a colder water community dominated approximately equally by copepods and euphausiids characterised the southern group. The macrozooplankton/nekton community is similarly responsive to regional primary productivity and chl-a patterns but our understanding of this community is to some degree limited by the depth of our sampling regime, which limits our interpretation to night-time stations. We find that *Thysanoessa* spp. is the dominant euphausiid in this region and that, based on our stratified net sampling strategy, *E. superba* was only a minor contributor to the off-shelf community biomass. Furthermore, myctophids appear widespread and may provide an alternative prey source for communities of higher predators on the SSI.

This paper forms a contribution to the British Antarctic Survey Ecosystems science programme.

Appendix A. Supplementary data

Supplementary data to this article can be found online at https://doi.org/10.1016/j.dsr2.2022.105073.

References

Achterberg, E.P., Moore, C.M., Henson, S.A., Steigenberger, S., Stohl, A., Eckhardt, S., Avendano, L.C., Cassidy, M., Hembury, D., Klar, J.K., Lucas, M.I., Macey, A.I., Marsay, C.M., Ryan-Keogh, T.J., 2013. Natural iron fertilization by the Eyjafjallajökull volcanic eruption. Geophys. Res. Lett. 40, 921–926.

Advisory Group to GSGSSI, 2018. SGSSI marine protected area 5-year review report to the Government of South Georgia and the South Sandwich Islands. https://www.gov.gs/docsarchive/search_all_documents/, 1-10.

Armand, L., Zielinski, U., 2001. Diatom species of the genus *Rhizosolenia* from Southern Ocean sediments: distribution and taxonomic notes. Diatom Res. 16, 259–294.

Atkinson, A., 1991. Life cycles of *Calanoides acutus, Calanus simillimus* and *Rhincalanus gigas* (Copepoda: Calanoida) within the Scotia Sea. Mar. Biol. 109, 79–91.

Atkinson, A., 1998. Life cycle strategies of epipelagic copepods in the Southern Ocean. J. Mar. Syst. 15, 289–311.

Atkinson, A., Siegel, V., Pakhomov, E., Rothery, P., Loeb, V., Ross, R., Quetin, L., Schmidt, K., Fretwell, P., Murphy, E., 2008. Oceanic circumpolar habitats of Antarctic krill. Mar. Ecol. Prog. Ser. 362, 1–23.

Atkinson, A., Ward, P., Williams, R., Poulet, S., 1992a. Feeding rates and diel vertical migration of copepods near South Georgia: comparison of shelf and oceanic sites. Mar. Biol. 114, 49–56.

Atkinson, A., Ward, P., Williams, R., Poulet, S.A., 1992b. Diel vertical migration and feeding of copepods at an oceanic site near South Georgia. Mar. Biol. 113, 583–593.

Baker, A.d.C., Clarke, M.R., Harris, M.J., 1973. The N.I.O. combination net (RMT 1 + 8) and further developments of rectangular midwater trawls. J. Mar. Biol. Assoc. U. K. 53, 167–184.

Bakker, D.C., Nielsdóttir, M.C., Morris, P.J., Venables, H.J., Watson, A.J., 2007. The island mass effect and biological carbon uptake for the subantarctic Crozet Archipelago. Deep-Sea Res. II: Top. Stud. Oceanogr. 54, 2174–2190.

Baldry, K., Strutton, P.G., Hill, N.A., Boyd, P.W., 2020. Subsurface chlorophyll-a maxima in the Southern Ocean. Front. Mar. Sci. 7, 671.

Browning, T., Bouman, H., Henderson, G., Mather, T., Pyle, D., Schlosser, C., Woodward, E., Moore, C., 2014. Strong responses of Southern Ocean phytoplankton communities to volcanic ash. Geophys. Res. Lett. 41, 2851–2857.

CCAMLR, 2021. Krill Fisheries. CCAMLR. https://www.ccamlr.org/en/fisheries/krill-fisheries.

Chitari, R.R., Anil, A.C., 2017. Estimation of diatom and dinoflagellate cell volumes from surface waters of the Northern Indian Ocean. Oceanologia 59, 389–395.

Clarke, K., Gorley, R., 2015. PRIMER V7: User Manual/Tutorial. PRIMER-E Plymouth.

Collins, M.A., Stowasser, G., Fielding, S., Shreeve, R., Xavier, J.C., Venables, H.J., Enderlein, P., Cherel, Y., Van de Putte, A., 2012. Latitudinal and bathymetric patterns in the distribution and abundance of mesopelagic fish in the Scotia Sea. Deep Sea Res. Part II Top. Stud. Oceanogr. 59–60, 189–198.

Convey, P., Morton, A., Poncet, J., 1999. Survey of marine birds and mammals of the South Sandwich Islands. Polar Rec. 35, 107–124.

de Baar, H.J.W., de Jong, J.T.M., Bakker, D.C.E., Löscher, B.M., Veth, C., Bathmann, U., Smetacek, V., 1995. Importance of iron for plankton blooms and carbon dioxide drawdown in the Southern Ocean. Nature 373, 412.

Dubischar, C., Lopes, R., Bathmann, U., 2002. High summer abundances of small pelagic copepods at the Antarctic Polar Front—implications for ecosystem dynamics. Deep-Sea Res. II: Top. Stud. Oceanogr. 49, 3871–3887.

Fetterer, F., Knowles, K., Meier, W.N., Savoie, M., Windnagel, A.K., 2017. Sea Ice index, version 3. NSIDC: national snow and ice data Centre. https://nsidc.org/data/G02135/versions/3.

Fielding, S., Stowasser, G., Ashurst, D., Apeland, B., Ariza, A., Baines, M., Cornwell, L., Hulbert, A., Jones-Williams, K., Lacey, C., Langan, E., Manno, C., Reichelt, M., McRae, E.D., Perry, F., Pinder, S., Rowlands, E., Saccomandi, F., Silvestri, C., Sorensen, M., Wynar, J., Leadbeater, A., Cheeseman, D., Harker, N., Moore, A., 2019. DY098 cruise report: polar Ocean ecosystem time series - western Core box. https://www.bodc.ac.uk/resources/inventories/cruise_inventory/report/17218/.

Fransz, H.G., Gonzalez, S.R., 1997. Latitudinal metazoan plankton zones in the Antarctic circumpolar current along 6°W during austral spring 1992. Deep-Sea Res. II: Top. Stud. Oceanogr. 44, 395–414.

Gallienne, C., Robins, D., 2001. Is *Oithona* the most important copepod in the world's oceans? J. Plankton Res. 23, 1421–1432.

GSGSSI, 2019. Government of South Georgia and the South Sandwich Islands marine protected areas order, 2019 (SR&O No 1 of 2019). In: GSGSSI (Ed.), 2. South Georgia and South Sandwich Islands Gazette, Falkland Islands, pp. 1–18.

Hagen, W., Kattner, G., 1998. Lipid metabolism of the Antarctic euphausiid *Thysanoessa macrura* and its ecological implications. Limnol. Oceanogr. 43, 1894–1901.

Hart, T., Convey, P., 2018. The South Sandwich Islands–a community of meta-populations across all trophic levels. Biodiversity 19, 20–33.

Holdgate, M., 1963. Observations in the South Sandwich islands, 1962. Polar Rec. 11, 394–405.

Holdgate, M.W., Baker, P.E., 1979. the South Sandwich Islands: I. General description. Sci. Rep. Br. Antarct. Surv. 91, 1–76.

Jiang, M., Measures, C.I., Barbeau, K.A., Charette, M.A., Gille, S.T., Hatta, M., Kahru, M., Mitchell, B.G., Naveira Garabato, A.C., Reiss, C., Selph, K., Zhou, M., 2019. Fe sources and transport from the Antarctic Peninsula shelf to the southern Scotia Sea. Deep-Sea Res. Part I Oceanogr. Res. Pap. 150, 103060.

Karakassis, I., Machias, A., Pitta, P., Papadopoulou, K.N., Smith, C.J., Apostolaki, E.T., Giannoulaki, M., Koutsoubas, D., Somarakis, S., 2006. Cross-community congruence of patterns in a marine ecosystem: do the parts reflect the whole? Mar. Ecol. Prog. Ser. 310, 47–54.

Karlson, B., Cusack, C., Bresnan, E., 2010. Microscopic and Molecular Methods for Quantitative Phytoplankton Analysis. UNESCO, Paris, France.

Kemp, S., Nelson, A.L., Tyrrell, G.W., 1931. The South Sandwich Islands, Cambridge.

Kiørboe, T., 2013. Zooplankton body composition. Limnol. Oceanogr. 58, 1843–1850.

Korb, R.E., Whitehouse, M.J., Thorpe, S.E., Gordon, M., 2005. Primary production across the Scotia Sea in relation to the physico-chemical environment. J. Mar. Syst. 57, 231–249.

Korb, R.E., Whitehouse, M.J., Ward, P., Gordon, M., Venables, H.J., Poulton, A.J., 2012. Regional and seasonal differences in microplankton biomass, productivity, and structure across the Scotia Sea: implications for the export of biogenic carbon. Deep-Sea Res. II: Top. Stud. Oceanogr. 59–60, 67–77.

Krafft, B.A., Macaulay, G.J., Skaret, G., Knutsen, T., Bergstad, O.A., Lowther, A., Huse, G., Fielding, S., Trathan, P., Murphy, E., Choi, S.-G., Chung, S., Han, I., Lee, K., Zhao, X., Wang, X., Ying, Y., Yu, X., Demianenko, K., Podhornyi, V., Vishnyakova, K., Pshenichnov, L., Chuklin, A., Shyshman, H., Cox, M.J., Reid, K., Watters, G.M., Reiss, C.S., Hinke, J.T., Arata, J., Godø, O.R., Hoem, N., 2021. Standing stock of antarctic krill (*Euphausia superba* Dana, 1850) (Euphausiacea) in the southwest Atlantic sector of the Southern Ocean, 2018–19. J. Crustac Biol. 41, 1–17.

Lancraft, T.M., Torres, J.J., Hopkins, T.L., 1989. Micronekton and macrozooplankton in the open waters near Antarctic ice edge zones (AMERIEZ 1983 and 1986). Polar Biol. 9, 225–233.

Lasbleiz, M., Leblanc, K., Armand, L.K., Christaki, U., Georges, C., Obernosterer, I., Quéguiner, B., 2016. Composition of diatom communities and their contribution to plankton biomass in the naturally iron-fertilized region of Kerguelen in the Southern Ocean. FEMS (Fed. Eur. Microbiol. Soc.) Microbiol. Ecol. 92.

Leakey, R.J.G., Leadbeater, B.S.C., Mitchell, E., McCready, S.M.M., Murray, A.W.A., 2002. The abundance and biomass of choanoflagellates and other nanoflagellates in waters of contrasting temperature to the north-west of South Georgia in the Southern Ocean. Eur. J. Protistol. 38, 333–350.

Leat, P.T., Fretwell, P.T., Tate, A.J., Larter, R.D., Martin, T.J., Smellie, J.L., Jokat, W., Bohrmann, G., 2016. Bathymetry and geological setting of the South Sandwich Islands volcanic arc. Antarct. Sci. 28, 293–303.

Leblanc, K., Arístegui, J., Armand, L., Assmy, P., Beker, B., Bode, A., Breton, E., Cornet, V., Gibson, J., Gosselin, M.-P., 2012. A global diatom database–abundance, biovolume and biomass in the world ocean. Earth Syst. Sci. Data 4, 149–165.

Liszka, C., NERC, 2021. In: Chlorophyll-a and Phaeopigment-A from RRS Discovery Southern Ocean Cruise DY098 to the Scotia Sea and South Sandwich Islands, during Austral Spring 2019 (Version 1.0). UK Polar Data Centre [Data set].

Liszka, C.M., Robinson, C., Manno, C., Stowasser, G., Tarling, G.A., 2021. Diel vertical migration of a Southern Ocean euphausiid, *Euphausia triacantha*, and its metabolic response to consequent short-term temperature changes. Mar. Ecol. Prog. Ser. 660, 37–52.

Lynch, H.J., White, R., Naveen, R., Black, A., Meixler, M.S., Fagan, W.F., 2016. In Stark contrast to widespread declines along the Scotia Arc, a survey of the South Sandwich Islands finds a robust seabird community. Polar Biol. 39, 1615–1625.

Martin, J.H., 1990. Glacial-interglacial CO_2 change: the iron hypothesis. Paleoceanography 5, 1–13.

Mathot, S., Smith Jr., W.O., Carlson, C.A., Garrison, D.L., Gowing, M.M., Vickers, C.L., 2000. Carbon partitioning within Phaeocystis Antarctica (Prymnesiophyceae) colonies in the Ross Sea, Antarctica. J. Phycol. 36, 1049–1056.

McGinty, N., Johnson, M.P., Power, A.M., 2014. Spatial mismatch between phytoplankton and zooplankton biomass at the Celtic Boundary Front. J. Plankton Res. 36, 1446–1460.

Murphy, E., Trathan, P., Everson, I., Parkes, G., Daunt, F., 1997. Krill fishing in the Scotia Sea in relation to bathymetry, including the detailed distribution around South Georgia. CCAMLR Sci. 4, 1–17.

Murphy, E.J., Watkins, J.L., Trathan, P.N., Reid, K., Meredith, M.P., Thorpe, S.E., Johnston, N.M., Clarke, A., Tarling, G.A., Collins, M.A., Forcada, J., Shreeve, R.S., Atkinson, A., Korb, R., Whitehouse, M.J., Ward, P., Rodhouse, P.G., Enderlein, P., Hirst, A.G., Martin, A.R., Hill, S.L., Staniland, I.J., Pond, D.W., Briggs, D.R., Cunningham, N.J., Fleming, A.H., 2007. Spatial and temporal operation of the Scotia Sea ecosystem: a review of large-scale links in a krill centred food web. Phil. Trans. R. Soc. B 362, 113–148.

Nissen, C., Vogt, M., 2021. Factors controlling the competition between *Phaeocystis* and diatoms in the Southern Ocean and implications for carbon export fluxes. Biogeosciences 18, 251–283.

Nordhausen, W., 1992. Distribution and growth of larval and adult *Thysanoessa macrura* (Euphausiacea) in the Bransfield Strait region, Antarctica. Mar. Ecol. Prog. Ser. 83, 185–196.

NSIDC, 2022. All about Sea Ice. National snow and ice data center. www.nsidc.org.

Park, Y.-H., Durand, I., SEANOE, 2019. In: Altimetry-drived Antarctic Circumpolar Current Fronts. https://www.seanoe.org/data/00486/59800/.

Pausch, F., Bischof, K., Trimborn, S., 2019. Iron and manganese co-limit growth of the Southern Ocean diatom *Chaetoceros debilis*. PLoS One 14, e0221959.

Perissinotto, R., Laubscher, R., McQuaid, C., 1992. Marine productivity enhancement around bouvet and the South Sandwich Islands (Southern Ocean). Mar. Ecol. Prog. Ser. 88, 41-41.

Petrou, K., Trimborn, S., Rost, B., Ralph, P.J., Hassler, C.S., 2014. The impact of iron limitation on the physiology of the Antarctic diatom Chaetoceros simplex. Mar. Biol. 161, 925–937.

Piatkowski, U., 1985. Distribution, abundance and diurnal migration of macrozooplankton in Antarctic surface waters. Meeresforschung-Rep. Mar. Res. 30, 264–279.

Piatkowski, U., Rodhouse, P.G., White, M.G., Bone, D.G., Symon, C., 1994. Nekton community of the Scotia Sea as sampled by the RMT25 during austral summer. Mar. Ecol. Prog. Ser. 112, 13–28.

Poulton, A.J., Mark Moore, C., Seeyave, S., Lucas, M.I., Fielding, S., Ward, P., 2007. Phytoplankton community composition around the Crozet Plateau, with emphasis on diatoms and *Phaeocystis*. Deep-Sea Res. II: Top. Stud. Oceanogr. 54, 2085–2105.

QGIS Development Team, 2020. QGIS Geographic Information System. Open Source Geospatial Foundation. http://qgis.org.

R Development Core Team, 2019. R: A Language and Environment for Statistical Computing, 3.6.2. R Foundation for Statistical Computing, Vienna, Austria.

Saunders, R.A., Collins, M.A., Foster, E., Shreeve, R., Stowasser, G., Ward, P., Tarling, G. A., 2014. The trophodynamics of Southern Ocean *Electrona* (Myctophidae) in the Scotia Sea. Polar Biol. 37, 789–807.

Saunders, R.A., Collins, M.A., Ward, P., Stowasser, G., Hill, S.L., Shreeve, R., Tarling, G. A., 2015a. Predatory impact of the myctophid fish community on zooplankton in the Scotia Sea (Southern Ocean). Mar. Ecol. Prog. Ser. 541, 45–64.

Saunders, R.A., Collins, M.A., Ward, P., Stowasser, G., Shreeve, R., Tarling, G.A., 2015b. Distribution, population structure and trophodynamics of Southern Ocean *Gymnoscopelus* (Myctophidae) in the Scotia Sea. Polar Biol. 38, 287–308.

Saunders, R.A., Hill, S.L., Tarling, G.A., Murphy, E.J., 2019. Myctophid fish (Family Myctophidae) are central Consumers in the food web of the Scotia Sea (Southern Ocean). Front. Mar. Sci. 6, 530.

Scott, F.J., Marchant, H.J., 2005. Antarctic Marine Protists. Australian Biological Resources Study Canberra.

Silk, J.R., Thorpe, S.E., Fielding, S., Murphy, E.J., Trathan, P.N., Watkins, J.L., Hill, S.L., 2016. Environmental correlates of antarctic krill distribution in the Scotia Sea and southern Drake passage. ICES J. Mar. Sci. 73, 2288–2301.

Singler, H.R., Villareal, T.A., 2005. Nitrogen inputs into the euphotic zone by vertically migrating *Rhizosolenia* mats. J. Plankton Res. 27, 545–556.

Tagliabue, A., Arrigo, K.R., 2003. Anomalously low zooplankton abundance in the Ross Sea: an alternative explanation. Limnol. Oceanogr. 48, 686–699.

Thorpe, S., Murphy, E., This issue. Spatial and temporal variability and connectivity of the marine environment of the South Sandwich Islands, Southern Ocean. Deep-Sea Res. II: Top. Stud. Oceanogr.

Trathan, P.N., Collins, M.A., Grant, S.M., Belchier, M., Barnes, D.K., Brown, J., Staniland, I.J., 2014. The South Georgia and the South Sandwich Islands MPA: protecting a biodiverse oceanic island chain situated in the flow of the Antarctic Circumpolar Current. Adv. Mar. Biol. 69, 15–78.

Tynan, E., Clarke, J.S., Humphreys, M.P., Ribas-Ribas, M., Esposito, M., Rérolle, V.M.C., Schlosser, C., Thorpe, S.E., Tyrrell, T., Achterberg, E.P., 2016. Physical and biogeochemical controls on the variability in surface pH and calcium carbonate saturation states in the Atlantic sectors of the Arctic and Southern Oceans. Deep-Sea Res. II: Top. Stud. Oceanogr. 127, 7–27.

Van de Putte, A.P., Van Houdt, J.K.J., Maes, G.E., Hellemans, B., Collins, M.A., Volckaert, F.A.M., 2012. High genetic diversity and connectivity in a common mesopelagic fish of the Southern Ocean: the myctophid *Electrona antarctica*. Deep-Sea Res. II: Top. Stud. Oceanogr. 59–60, 199–207.

Venables, H.J., Clarke, A., Meredith, M.P., 2013. Wintertime controls on summer stratification and productivity at the western Antarctic Peninsula. Limnol. Oceanogr. 58, 1035–1047.

Villareal, T.A., Pilskaln, C.H., Montoya, J.P., Dennett, M., 2014. Upward nitrate transport by phytoplankton in oceanic waters: balancing nutrient budgets in oligotrophic seas. PeerJ 2 e302-e302.

Wallis, J.R., Maschette, D., Wotherspoon, S., Kawaguchi, S., Swadling, K.M., 2020. *Thysanoessa macrura* in the southern Kerguelen region: population dynamics and biomass. Deep-Sea Res. II: Top. Stud. Oceanogr. 174, 104719.

Ward, P., Atkinson, A., Murray, A., Wood, A., Williams, R., Poulet, S., 1995. The summer zooplankton community at South Georgia: biomass, vertical migration and grazing. Polar Biol. 15, 195–208.

Ward, P., Atkinson, A., Tarling, G., 2012. Mesozooplankton community structure and variability in the Scotia Sea: a seasonal comparison. Deep-Sea Res. II: Top. Stud. Oceanogr. 59–60, 78–92.

Ward, P., Grant, S., Brandon, M., Siegel, V., Sushin, V., Loeb, V., Griffiths, H., 2004. Mesozooplankton community structure in the Scotia Sea during the CCAMLR 2000 survey: January–February 2000. Deep-Sea Res. II: Top. Stud. Oceanogr. 51, 1351–1367.

Ward, P., Shreeve, R., Whitehouse, M., Korb, B., Atkinson, A., Meredith, M., Pond, D., Watkins, J., Goss, C., Cunningham, N., 2005. Phyto- and zooplankton community structure and production around South Georgia (Southern Ocean) during Summer 2001/02. Deep-Sea Res. Part I Oceanogr. Res. Pap. 52, 421–441.

Ward, P., Whitehouse, M., Brandon, M., Shreeve, R., Woodd-Walker, R., 2003. Mesozooplankton community structure across the antarctic circumpolar current to the north of South Georgia: southern Ocean. Mar. Biol. 143, 121–130.

Ward, P., Whitehouse, M., Shreeve, R., Thorpe, S., Atkinson, A., Korb, R., Pond, D., Young, E., 2007. Plankton community structure south and west of South Georgia (Southern Ocean): links with production and physical forcing. Deep-Sea Res. Part I Oceanogr. Res. Pap. 54, 1871–1889.

Watkins, J.L., Hewitt, R., Naganobu, M., Sushin, V., 2004. The CCAMLR 2000 Survey: a multinational, multi-ship biological oceanography survey of the Atlantic sector of the Southern Ocean. Deep-Sea Res. II: Top. Stud. Oceanogr. 51, 1205–1213.

Whitehouse, M.J., Korb, R.E., Atkinson, A., Thorpe, S.E., Gordon, M., 2008. Formation, transport and decay of an intense phytoplankton bloom within the High-Nutrient Low-Chlorophyll belt of the Southern Ocean. J. Mar. Syst. 70, 150–167.

Yentsch, C.S., Menzel, D.W., 1963. A method for the determination of phytoplankton chlorophyll and phaeophytin by fluorescence. Deep-Sea Res. Oceanogr. Abstr. 10, 221–231.